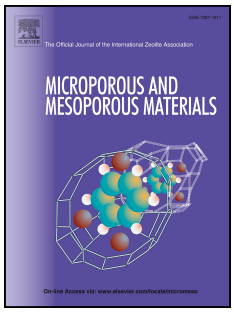

Mesoporous configuration effects on the physicochemical features of hierarchical ZSM-5 supported cobalt oxide as catalysts in methane partial oxidation

Irena Khatrin, Iman Abdullah, Alan J. McCue, Yuni K. Krisnandi

PII: S1387-1811(23)00472-9

DOI: https://doi.org/10.1016/j.micromeso.2023.112896

Reference: MICMAT 112896

To appear in: *Microporous and Mesoporous Materials*

Received Date: 13 August 2023

Revised Date: 7 November 2023

Accepted Date: 8 November 2023

Please cite this article as: I. Khatrin, I. Abdullah, A.J. McCue, Y.K. Krisnandi, Mesoporous configuration effects on the physicochemical features of hierarchical ZSM-5 supported cobalt oxide as catalysts in methane partial oxidation, *Microporous and Mesoporous Materials* (2023), doi: https://doi.org/10.1016/j.micromeso.2023.112896.

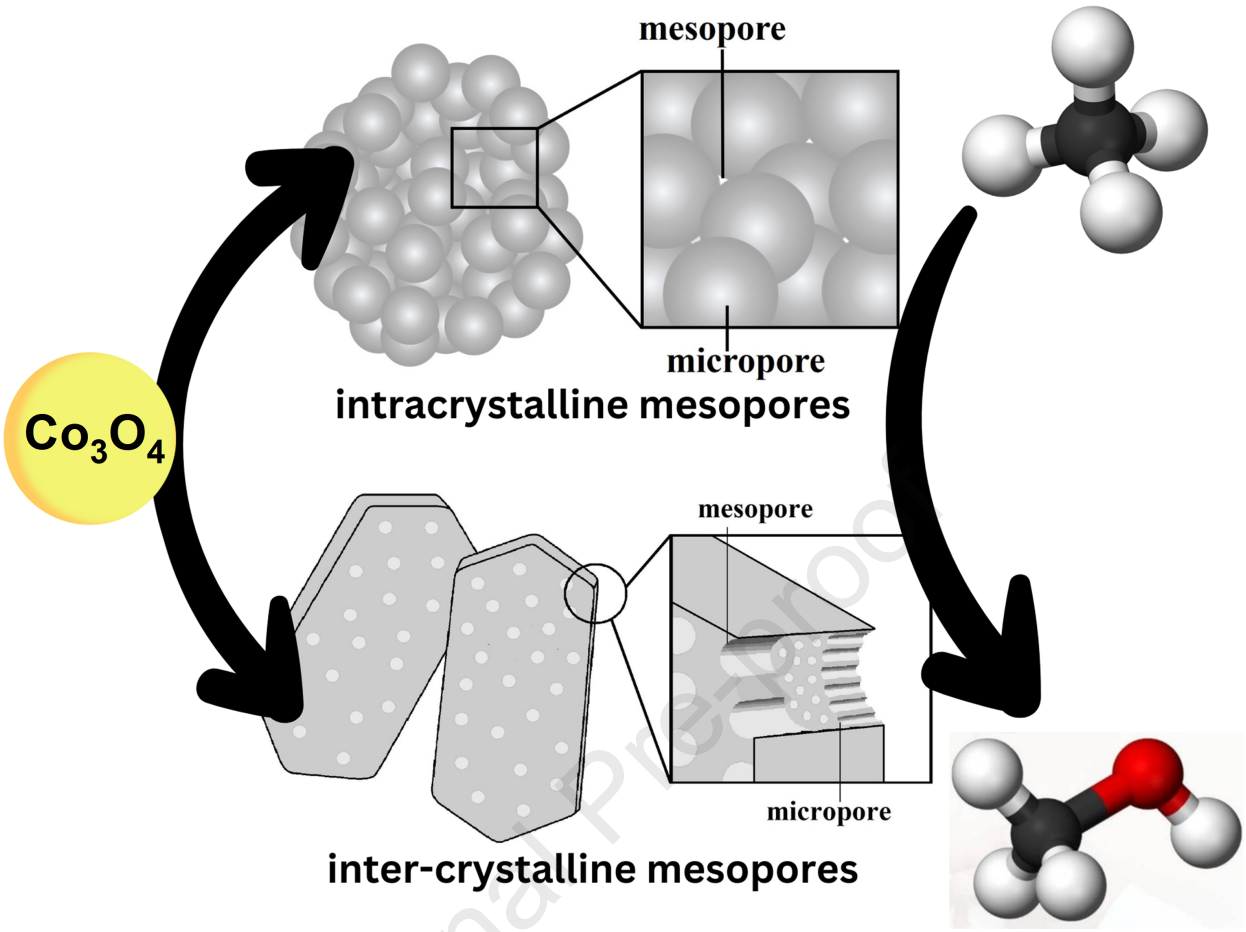

Mesoporous Configuration Effects on The Physicochemical Features of Hierarchical ZSM-5 Supported Cobalt Oxide as Catalysts in Methane Partial Oxidation

Irena Khatrin[a,b], Iman Abdullah[a,b], Alan J. McCue[c], Yuni K. Krisnandi[a,b,*]

[a] Department of Chemistry, Faculty of Mathematics and Natural Sciences Universitas Indonesia, Kampus UI Depok, Depok 16424, Indonesia

[b] Solid Inorganic Framework Laboratory, Department of Chemistry, Faculty of Mathematics and Natural Sciences Universitas Indonesia, Depok 16424, Indonesia

[c] Department of Chemistry, University of Aberdeen, Aberdeen AB24 3UE, UK

*Corresponding author: yuni.krisnandi@sci.ui.ac.id

Abstract:

Hierarchical porous system has become a prevalent method to overcome the diffusion limitation of conventional zeolites. Two types of mesopores characterized as intra-crystalline (mesopores in the zeolite pore wall) and inter-crystalline mesopores (meso-sized voids between nano-zeolite aggregates) could be formed in the synthesis of hierarchical zeolites. In an attempt to investigate the influence of mesopores structure on the physicochemical properties of hierarchical ZSM-5, specifically cobalt oxide impregnated ZSM-5 zeolite samples with intra- and inter-crystalline mesopores were synthesized through two different synthesis strategies. Analysis of the physicochemical properties of the as-modified hierarchical ZSM-5 catalysts were carried out using SEM, TEM, XPS, and H_2-TPR which showed distinct features given by the two mesopores configurations. Co-oxide impregnated on ZSM-5 with inter-crystalline mesopores was dominated by Co(II) species, while Co-oxide/ZSM-5 showed a fair amount of Co(III) and Co(II). Furthermore, analysis of the catalytic activity was conducted using methane partial oxidation as a model reaction. With a variation in reaction time, various types of oxygenated products, i.e. methanol, formaldehyde, formic acid, and a small trace of carbon dioxide were observed. Catalytic results suggested that the Co-oxide/ZSM-5 material with inter-crystalline mesopores configuration is more active for the methane partial oxidation reaction compared to the Co-oxide/ZSM-5 with intracrystalline mesopores. This was

confirmed by the formation of formaldehyde rather than methanol as the major product in the brief reaction time of 30 mins.

Keywords:

hierarchical ZSM-5; mesopores configuration; intra- and inter-crystalline mesopores; Co-oxide ZSM-5; methane partial oxidation.

1. Introduction

ZSM-5 zeolite offers promising catalytic performance in various notable reactions, such as pyrolysis [1], oxidation [2], dehydroaromatization [3], and oligomerization [4] which require the molecular-sieve feature of the abundant ZSM-5 micropores that often leads to the diffusion limitation and degradation of catalyst activity, efficiency, and selectivity [5]. Several efforts have been made to lessen the diffusion restriction, such as altering the morphology of the zeolite into nano-sized particles and/or creating hierarchical zeolites [6]. Wang *et al*. reported that the particle morphology of ZSM-5 with varied porous structures significantly altered the acid distribution and zeolite interaction with cobalt oxide which could effectively advance the production of diesel oil. More cobalt-zeolite support interactions were shown by smaller ZSM-5 particles with stronger acid sites [7]. However, nano-sized zeolites are often tightly agglomerated, and this causes structural instability, making hierarchical zeolite a prevalent method to overcome the diffusion limitation, which combines two approaches of enlarging the pore size and reducing the diffusion pathway [8].

Hierarchical zeolite features wider integrated secondary pore systems (>2 nm) as access to the microporous active sites. Pérez-Ramírez *et al*. demonstrated that the hierarchical pore system could be attained through three types of zeolite synthesis: (i) nano-zeolite, (ii) zeolite composite and (iii) mesoporous zeolite [9]. Furthermore, two types of mesopores characterized as intracrystalline and inter-crystalline mesopores could be formed in the synthesis of hierarchical zeolites. Based on our previous work, the intracrystalline mesopores are defined as ordered mesopores within the pore walls of a zeolite, that could be synthesized through a dual-template method. On the other hand, inter-crystalline mesopores are regarded as disordered meso-sized voids within nano-zeolite aggregates, that could be synthesized through a template-free method [10]. The physicochemical property differences between the two mesopore types of hierarchical H-ZSM-5 affected the catalytic properties for LDPE cracking,

where H-ZSM-5 with inter-crystalline mesopores performed better than intracrystalline H-ZSM-5 despite its lower amount of acid sites [10].

The methane oxidation reaction can occur *via* two methods: steam reforming to synthetic gas or partial oxidation reaction to high-value chemicals or precursors [11]. However, the partial oxidation reaction which directly converts methane into valuable chemicals is preferred in terms of time, cost- and energy efficiency [12]. Three types of oxygenated products result from methane partial oxidation reaction, including methanol, formaldehyde, and formic acid which vary in molecular size. Methanol is desirable as the main product of methane partial oxidation, as it is known as a precursor to many high-value chemicals such as formaldehyde and propylene [13].

In order to investigate the influence of mesopore structure on the physicochemical properties of hierarchical ZSM-5 specifically modified with cobalt oxide, ZSM-5 zeolite with intra- and inter-crystalline mesopores were synthesized. It is believed that the variation of mesopore configuration could alter the properties of hierarchical ZSM-5 supported with cobalt oxide. For instance, in terms of porosity, metal active sites, and its acidity properties in the methane partial oxidation that could result in a variety of oxygenated products, making it worthwhile to study. To the best of our knowledge, this kind of study has not yet been reported to date and can hopefully contribute to the industrial process that has widely utilized metal-oxide-supported hierarchical zeolite [14–17]. A series of characterization methods including Scanning Electron Microscope (SEM), Transmission Electron Microscope (TEM), X-ray Photoelectron Spectroscopy (XPS), and H_2-Temperature Programmed Reduction (H_2-TPR) were implemented to understand the physicochemical properties of as-modified ZSM-5. Furthermore, their properties were evaluated based on the catalytic performance in the methane oxidation reaction as a model reaction.

2. Experimental

2.1. Materials

Sodium aluminate ($NaAlO_2$), tetraethyl orthosilicate (TEOS, 98%), tetrapropylammonium hydroxide (TPAOH 40 wt. %), poly(diallyldimethylammonium) chloride (PDDA, 20 wt. %), and tetrapropylammonium Bromide (TPABr, 98%) were purchased from Sigma Aldrich. Glacial acetic acid, cobalt(II) nitrate hexahydrate, sodium hydroxide (NaOH 50% w/v), and ethanol were purchased from Merck. Ultra-high purity methane and a mixture of N_2:O_2 (0.5%)

gas were purchased from PT Aneka Gas Industri. Including deionized water, all materials were of reagent grade and utilized without any purification treatment.

2.2. Synthesis of Hierarchical Co_3O_4/ZSM-5

2.2.1. Templating Method

Hierarchical ZSM-5 with intracrystalline mesopores was prepared *via* the hydrothermal method following our previous work [10]. TPAOH and PDDA were used as the templates, along with sodium aluminate and TEOS as alumina and silica sources, respectively. The materials were mixed with a molar ratio of 1.0 Al_2O_3: 64.3 SiO_2: 10.1 $(TPA)_2O$: 3571.7 H_2O at 100 °C and pH 11. The homogeneous mixture was stirred and kept at room temperature for 48 h before being moved to an autoclave for the crystallization process at 170 °C for 144 h. The obtained solid was filtered and washed to pH 7 before being dried in the oven at 60 °C overnight. The samples were then calcined in static air at 550 °C for 3 h to afford a sample denoted as 'ZHT'.

2.2.2. Mesoporogen-free Method

Hierarchical ZSM-5 with inter-crystalline mesopores was prepared following the mesoporogen-free method of Kadja *et al*. [18] at low-temperature. Synthesis was performed at room temperature with a molar ratio of 1 SiO_2 : 0.004 Al_2O_3 : 0.19 TPABr : 0.12 NaOH : 8 H_2O using sodium aluminate as an alumina source, Ludox HS-40 as silica source, NaOH and TPABr as a single template without the presence of mesoporogen. The mixture was stirred in a polypropylene bottle and directly crystallized in an oven at 90 °C for 96 h. The obtained solid was washed, dried at 100 °C overnight, and calcined at 550 °C for 6 h to afford a sample denoted as 'ZLT'.

2.2.3. Modification Co_3O_4/ZSM-5

Hierarchical Co_3O_4/ZSM-5 catalysts were prepared by the impregnation method. Specifically, 0.2495 M $Co(NO_3)_2 \cdot H_2O$ was added to ZHT or ZLT to give either a 2.5% or 5% molar ratio. The solution was stirred at room temperature to obtain a paste and then dried at 60 °C for 12 h before being calcined in static air at 550 °C for 3 h. The modified hierarchical ZSM-5 were labelled as Co_3O_4/ZHT2.5, Co_3O_4/ZHT5, Co_3O_4/ZLT2.5 and Co_3O_4/ZLT5.

2.3. Catalyst Characterization

Structure and crystallinity of the as-synthesized hierarchical ZSM-5 catalysts were analyzed using the XRD patterns collected on PANanlytical Empyrean X-ray diffractometer

operated at 40 kV and 30 mA, with Cu Kα (λ = 1.54059 Å) radiation in the 2θ range of 5–80°. The functional groups were analyzed by an Alpha-Bruker Fourier Transform Infrared spectrometer (FTIR) using the KBr pellet method and a spectral resolution of 4 cm^{-1}. X-Ray Fluorescence (XRF) analyses were performed on a PANanlytical ε1 instrument operated at 50 kV with Ag as the radiation source. Surface area analysis of N_2 physisorption was performed on a Quantachrome Quadrasorb-Evo surface area and pore size analyzer at –196.15 °C. Samples were degassed at 300 °C prior to measurement. Analysis was performed using Quantachrome NovaWin – Data Acquisition and Reduction application for NOVA instruments. The specific surface area was determined using the Brunauer–Emmett–Teller (BET), micropore volume was determined using the t-plot method, while Pore Size Distribution (PSD) was determined using the Barrett–Joyner–Halenda (BJH) method from the desorption branch. The total pore volume was analyzed based on N_2 adsorbed at a relative pressure $p/p_0 = 0.99$. The surface morphology of the samples was evaluated using a JEOL JSM-6510LA Scanning Electron Microscopy (SEM) and a TEM H9500 Transmission Electron Microscopy (TEM) instrument. X-ray Photoelectron Spectroscopy (XPS) was performed on Thermo Fisher Scientific K-alpha instrument using an Al Kα monochromator. Temperature Programmed Reduction (TPR) was performed on a Micromeritics Chemisorb 2720 instrument using 5% H_2/N_2 (20 mL min^{-1}) within the temperature range of 40 to 1000 °C at a heating rate of 10 °C min^{-1}.

2.4. Catalytic Test

Methane partial oxidation reactions were carried out in an atmospheric fixed-batch reactor at 150 °C with 0.5 g catalyst. The reactor was first flushed with N_2 prior to analysis and then 0.75 bar CH_4 and 2 bar N_2 (0.5% O_2) were added simultaneously. After catalytic tests were carried out for 30, 60, 90, and 120 min, reactor outlet gas was analyzed using a Shimadzu TCD-8A Gas Chromatography (GC) instrument equipped with PorapakQ column and thermal conductivity detector. The adsorbed products were extracted from the catalyst using 3 mL ethanol and analyzed offline using a Shimadzu FID-2014 GC instrument equipped with a RTX-1 carbowax column and flame ionization detector. The conversion of methane and the yield of products were determined according to the following equations:

$$CH_4 \text{conversion } (\%) = \frac{([CH_4]_{inlet} - [CH_4]_{outlet})}{[CH_4]_{inlet}} \times 100\% \quad (1)$$

$$\text{Product yield } (\%) = \frac{[Product]_{outlet}}{[CH_4]_{inlet}} \times 100\% \quad (2)$$

3. Results and Discussion

3.1. Catalyst Characterization

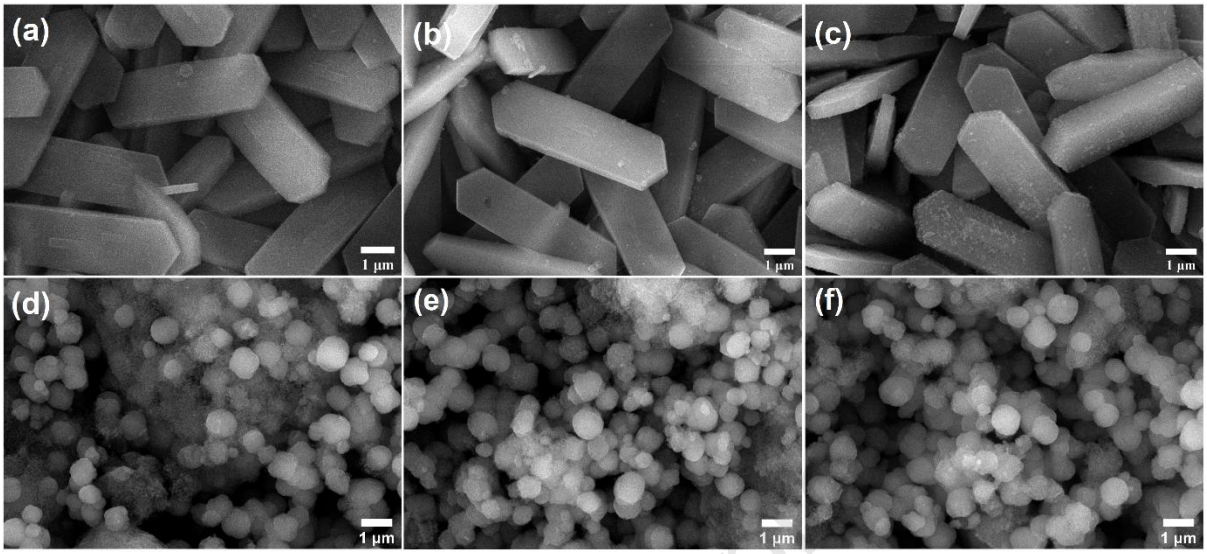

Fig. 1. SEM images of (a) ZHT, (b) Co_3O_4/ZHT2.5, (c) Co_3O_4/ZHT5, (d) ZLT, (e) Co_3O_4/ZLT2.5, and (f) Co_3O_4/ZLT5.

The morphology and microstructure of ZSM-5 catalysts were analyzed by SEM characterization. Fig. 1a reveals the hexagonal coffin-shaped ZHT particles, characteristic of a MFI-type zeolite (4.8 μm) with a relatively smooth surface morphology indicating high crystallinity which is also implied by XRD analysis (see later) [19]. On the other hand, ZLT samples in Fig. 1d reveal a granular spherical morphology (0.8 μm) as the common structure of ZSM-5 zeolite synthesized in the absence of an Organic Structure Directing Agent (OSDA) [20]. Furthermore, the Scherrer analysis method of crystallite size determination reveals that ZLT consists of nano-zeolite aggregates in the size of 19 nm.

No morphology changes in hierarchical ZSM-5 structure were observed after the addition of cobalt precursor or with increasing loading of cobalt. The modification by cobalt oxide is shown by the presence of small white particles deposited randomly on the crystal surface of ZHT (Fig. 1b,c) after the impregnation process with intensity increasing with the increment of percent loading [21]. However, the same condition is not observed on ZLT (Fig. 1e,f) which suggests better dispersion of nano Co_3O_4 on the surface of ZLT nanocrystallites, in agreement with the increase of S_{BET} after impregnation of cobalt oxides [22].

The XRD patterns of hierarchical ZSM-5 and Co_3O_4/ZSM-5 catalysts are presented in Fig. 2. All ZHT and ZLT catalysts exhibit similar characteristic peaks as the ZSM-5 reference at 2θ of 7.9, 8.8, 23.1, 23.9, and 24.3° [23], indicating the formation of the MFI framework structure

(based on JCPDS 44-0003) [24–26]. The degree of crystallinity was determined based on the peak intensity of the characteristic peaks at 2θ of 21–26° according to the ASTM D5758-01 method [27,28]. The ZHT sample which was synthesized through a templating method possesses the highest intensity compared to ZLT and is therefore considered to have a crystallinity degree of 100%.

After modification with Co_3O_4, in general, the structure of both ZHT and ZLT was preserved, as shown by the existence of the characteristic peaks of MFI in the XRD patterns. In addition, modifications led to the creation of several new peaks at 2θ of 31.3, 36.8, 59.3, and 65.2° corresponding to (220), (311), (511), and (440) planes of Co_3O_4 with spinel structure (JCPDS 42-1467) [29]. The Co_3O_4 spinel as the single phase was confirmed by the absence of peaks associated with CoO and Co_2O_3 (i.e., 2θ = 42.6°, 61.8°, and 22.1°) (JCPDS 01-1227) [30,31]. On the other hand, modification with Co_3O_4 was observed to decrease the catalyst crystallinity as the Co_3O_4 ratio increased. It is worth noting that the crystallinity of Co_3O_4/ZLT was better preserved than Co_3O_4/ZHT. These results indicate that the insertion process of metal species into the zeolite micropore system at elevated temperature (550 °C) has affected the ZSM-5 framework structure [32,33]. Therefore, to confirm this effect, the lattice parameters of modified hierarchical ZSM-5 were calculated to identify any structural changes following the orthorhombic symmetry formula in Eq. 3 and listed in Table 1 [34].

$$\frac{\sin\theta}{\lambda} = \frac{\sqrt{(hbc)^2+(kca)^2+(lab)^2}}{2\,abc} \quad (3)$$

The results showed that the *a* and *c* values of modified ZHT increased while the *b* value decreased. Conversely, the *a*, *b*, and *c* values of modified ZLT seem to decrease compared to the parent ZSM-5 values that exhibit the same results as reported by Kokotailo *et al*. [35]. The change of the lattice parameter values is accompanied by the slight shift of ZSM-5 characteristic peaks to higher 2θ for modified ZHT and lower 2θ for ZLT. Guan *et al*. reported similar work on the Co/ZSM-5 preparation *via* impregnation suggested that these results could be due to the substitution of the Al^{3+} in the ZSM-5 framework with cobalt species from the $Co(NO_3)_2 \cdot H_2O$ precursor, which led to the adjustment of lattice parameters but does not change the overall structure [36]. Scherrer's equation was used to estimate the Co_3O_4 crystallite size. The calculation results (also shown in Table 1) show that the Co_3O_4 particle size on Co_3O_4/ZHT became more significant with increased Co loading. Meanwhile, interestingly, the Co_3O_4 particle size on the Co_3O_4/ZLT decreased with an increase in Co loading.

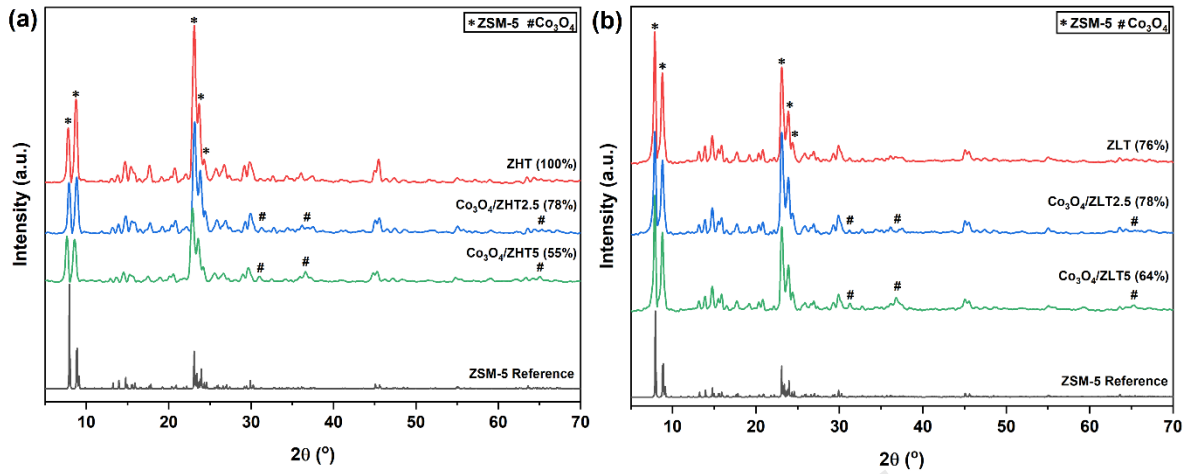

Fig. 2. XRD patterns of (a) ZHT, (b) ZLT, and their modified Co_3O_4 derivatives with the degree of crystallinity.

Table 1. Unit cell parameters of ZSM-5 catalysts and Co_3O_4 crystallite size.

Catalyst	*a* (Å)	*b* (Å)	*c* (Å)	Co_3O_4 size (nm)
ZHT	20.02	19.90	13.38	-
Co_3O_4/ZHT2.5	20.23	19.87	13.69	16
Co_3O_4/ZHT5	20.03	19.80	13.48	20
ZLT	20.38	19.85	13.78	-
Co_3O_4/ZLT2.5	20.14	19.78	13.53	25
Co_3O_4/ZLT5	20.12	19.77	13.53	22

FTIR spectra of all hierarchical ZSM-5 and their derivatives are presented in Fig. 3. The broad bands at 4000–3000 cm^{-1} are attributed to the stretching vibration of silanol (Si–OH) groups. It can be seen that the band in ZHT and the modified Co_3O_4 derivatives (Fig. 3a) consist of two peaks at 3640 cm^{-1} and 3453 cm^{-1}, indicating the presence of both isolated and hydrogen-bonded silanol groups, respectively. The peak at 3453 cm^{-1} could also be attributed to the Al–OH in the ZSM-5 framework that works as Bronsted acid sites [37]. Meanwhile, the band in ZLT and the modified Co_3O_4 derivatives (Fig. 3b) are primarily made up of hydrogen-bonded silanol groups.

Fig. 3 also shows that all catalysts exhibit five typical zeolite peaks in the wavenumber range of 1600–500 cm^{-1}. Both peaks at 1070 cm^{-1} and 790 cm^{-1} are attributed to the external symmetric stretching mode [38]. While peaks at 1220 cm^{-1} and 550 cm^{-1} are attributed to the asymmetric stretching of T–O–T (within TO_4 tetrahedra, T = Si, Al) and vibration of distorted double five-membered-ring of ZSM-5, respectively [39,40]. A peak at 1610 cm^{-1} is ascribed to adsorbed H_2O [41]. These results support XRD results and confirm the successful synthesis

of the hierarchical ZSM-5 molecular framework. With respect to the intensity of all peaks typical of the zeolites, it can be seen that the intensity in the ZHT-supported catalysts tends to increase after modification with Co_3O_4, while ZLT-supported catalysts decrease after modification with Co_3O_4. The difference in the silanol group content and characteristic peak intensity highlights the potential for distinct physicochemical features across each hierarchical ZSM-5 mesopore configuration.

Furthermore, spectra of ZHT and ZLT in Fig. 3 also showed two additional peaks after modification with Co_3O_4 at 670 cm^{-1} and 595 cm^{-1} which are assigned to the stretching vibration of Co^{3+}–O and Co^{2+}–O species of Co_3O_4 [42,43]. It is also observed that peak intensity increases as the metal loading increases, which agress with XRD results.

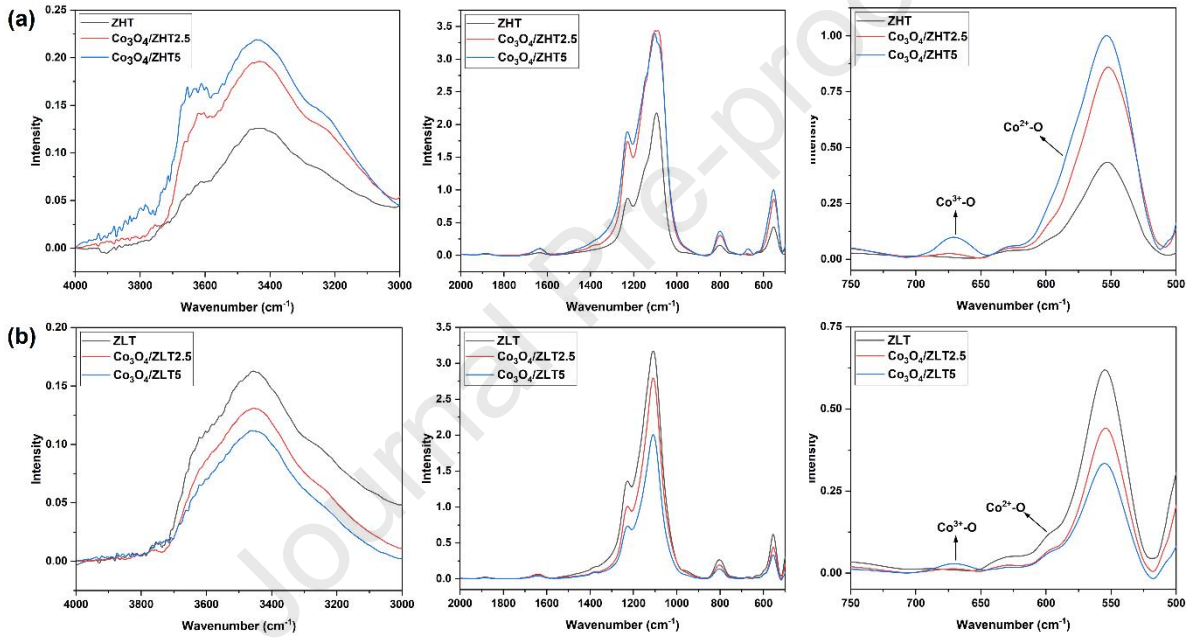

Fig. 3. FTIR spectra of (a) ZHT, (b) ZLT catalysts and their modified Co_3O_4 derivatives.

X-ray fluorescence measurement results presented in Table 2 showed the Si/Al ratio of the as-synthesized ZHT and ZLT samples are 59 and 74, respectively. No changes in the Si/Al ratio after modification with Co-oxide indicates that the impregnation process did not cause dealumination or desilication of ZSM-5 [44]. Actual cobalt loading of 2.5 and 5 wt.% were determined by XRF and are consistent with the theoretical value indicating the successful metal deposition into hierarchical ZSM-5.

The N_2 adsorption-desorption isotherm presented in Fig. 4(a) shows a hysteresis loop at $p/p_0 > 0.4$ corresponding to capillary condensation in the hierarchical system in both ZSM-5 catalysts [45]. However, ZHT and ZLT possess different types of hysteresis loops. ZHT which is synthesized through the templating method exhibits a type H4 hysteresis loop where the

increment of the adsorption-desorption curve happened gradually in the relatively small silt-like pore (~ 2 nm) [46]. Meanwhile, ZLT which is synthesized through the mesoporogen-free method exhibits a type H3 hysteresis loop with significant increment at $p/p_0 > 0.9$ suggesting that capillary condensation happens in the stack of nano-zeolite aggregates which often leads to the creation of inter-crystalline mesopores [47–49]. The parallel assembly of adsorption-desorption isotherm curves verifies the interconnected pore system to the surface of hierarchical ZSM-5 [50]. Moreover, modification of hierarchical ZSM-5 with Co_3O_4 showed a similar isotherm curve with the pristine ZSM-5 parents, which is in agreement with the XRD results, where no alteration of the framework structure of ZSM-5 occurred after impregnation [51]. Textural properties of as-synthesized hierarchical ZSM-5 are presented in Table 2. ZHT exhibits a higher total surface area (S_{BET} and S_{ext}) compared with ZLT, which might be due to the synthesis method of ZLT which doesn't include the presence of a mesoporogen.

The hierarchy system plays an important role in molecular transport in the catalytic process [52]. Therefore, a thorough analysis of the porosity of the as-synthesized ZHT and ZLT was carried out using the eminent descriptor of HF (Hierarchical Factor) based on Eq. 4:

$$HF = \left(\frac{V_{micro}}{V_{total}}\right) \times \left(\frac{S_{meso}}{S_{BET}}\right) \quad (4)$$

Peréz-Ramírez et al. in their study, identified hierarchical zeolites as materials with HF value > 0.10 which suggests that both ZHT and ZLT are hierarchical zeolites (Table 2). Modification of ZHT with Co_3O_4 resulted in lower S_{BET} and V_{micro} values and an increase of V_{meso} which might suggest the aggregation of cobalt oxides and/or pore blocking [21]. Conversely, S_{BET} of Co_3O_4/ZLT increases compared to the parent ZLT which indicates that the cobalt oxide does not block the pore and is more evenly dispersed across the surface of ZLT [53].

Determination of pore size was carried out using the BJH method for analysis of mesopore size [54]. Pore size distribution of ZHT (Fig. 3a) revealed a uniform mesoporous size of about 2 nm with a slight decrease after impregnation with Co_3O_4. Whereas ZLT revealed a bimodal mesopore size distribution in the size of 2–3 nm and 26–35 nm which might result due to the lack of a mesopore structure directing agent in the synthesis method [55]. As reflected in the pore size distribution of ZHT and ZLT after modification with Co_3O_4, there was a slight decrease in the pore size which was also observed on the isotherm curve indicating a small amount of cobalt oxide particle blocked the ZSM-5 pores.

Table 2. Compositional and textural properties of ZHT and ZLT, as well as their modified Co_3O_4 derivatives.

Catalyst	XRF		N_2 physisorption							
	Si/Al	Co	S_{BET} [m^2/g][a]	S_{micro} [m^2/g][b]	S_{ext} [m^2/g][b]	V_{total} [cm^3/g][c]	V_{micro} [cm^3/g][b]	V_{meso} [cm^3/g][b]	HF	Pore diameter (nm)[d]
ZHT	59	–	407	141	265	0.09	0.08	0.01	4.68	2.24
Co_3O_4/ZHT2.5	57	2.4	367	138	229	0.10	0.06	0.04	0.85	2.11
Co_3O_4/ZHT5	59	4.9	317	102	215	0.07	0.05	0.02	1.60	2.00
ZLT	74	–	265	190	75	0.28	0.08	0.20	0.12	2.64; 34.12
Co_3O_4/ZLT2.5	74	2.4	277	189	88	0.25	0.07	0.18	0.13	2.64; 26.72
Co_3O_4/ZLT5	74	4.8	270	193	77	0.22	0.07	0.15	0.14	2.64; 26.68

[a] Determined using BET method.
[b] Determined using *t*-plot method.
[c] Determined at $p/p_0 = 0.99$.
[d] Determined using BJH.

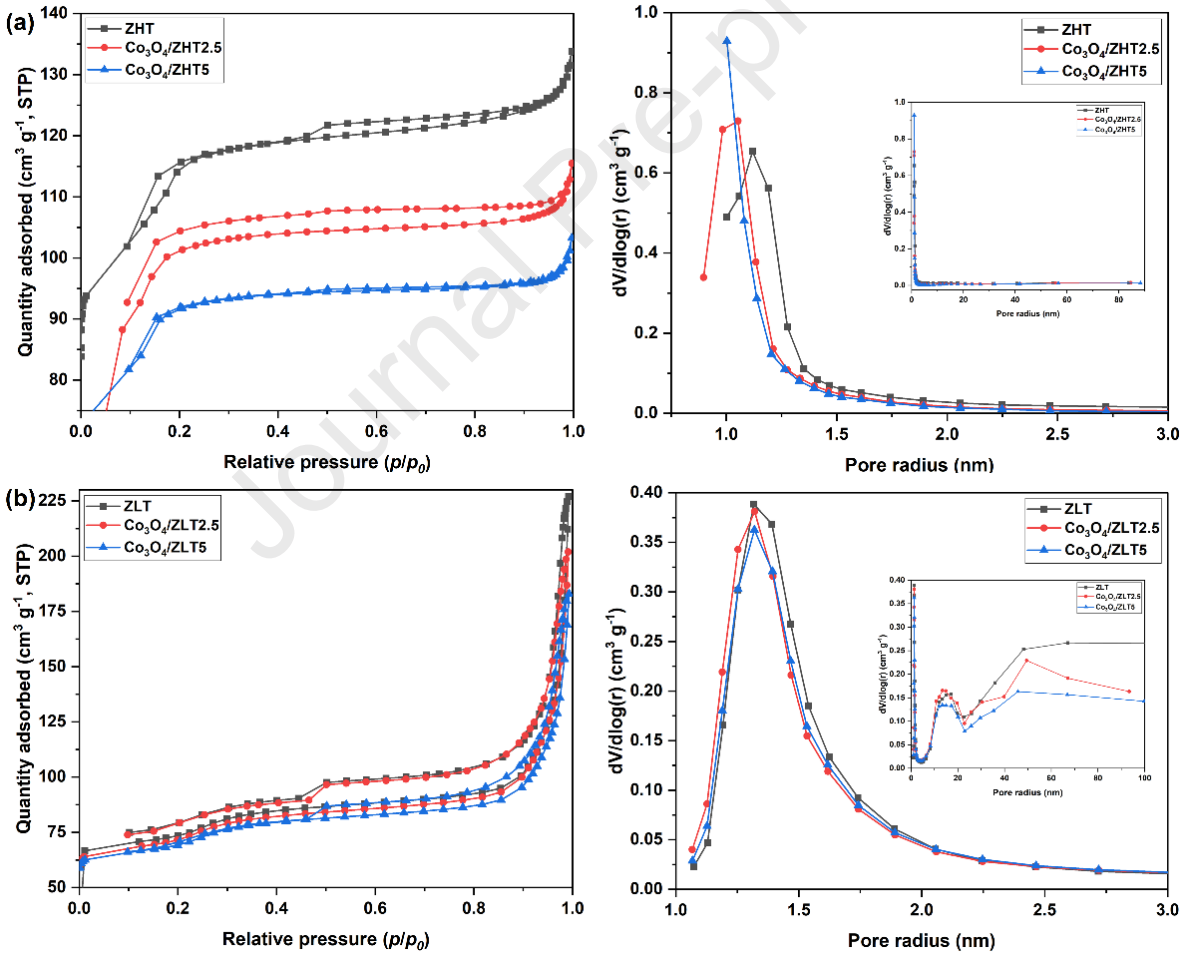

Fig. 4. (a) N_2 adsorption–desorption isotherm and (b) Pore size distribution of hierarchical ZSM-5 and Co_3O_4/ZSM-5.

TEM analysis was carried out to confirm the morphology and pore structure of the as-synthesized hierarchical ZSM-5 catalysts. Fig. 5a shows the morphology of ZHT with some intracrystalline mesopores, while the morphology of ZLT with inter-crystalline mesopores is shown in Fig. 5d. This result is similar to the configuration that was reported in our previous work [10]. There were also some defects observed on the ZHT structure due to the template removal process at high temperatures [50].

The impregnated Co_3O_4 presents as black spots on the surface of the zeolite in the TEM images. Compared to Co_3O_4/ZLT, the Co_3O_4 particle spots are hardly observed on the Co_3O_4/ZHT, which might be due to the insertion of Co_3O_4 particles into the ZHT support pore system, as indicated by the decrease of BET surface area (S_{BET}) and V_{micro}. Moreover, Co_3O_4 particle distribution on the ZLT surface is considered more well-dispersed compared to modified ZHT, therefore confirming the increment of ZLT BET surface area after impregnation [56].

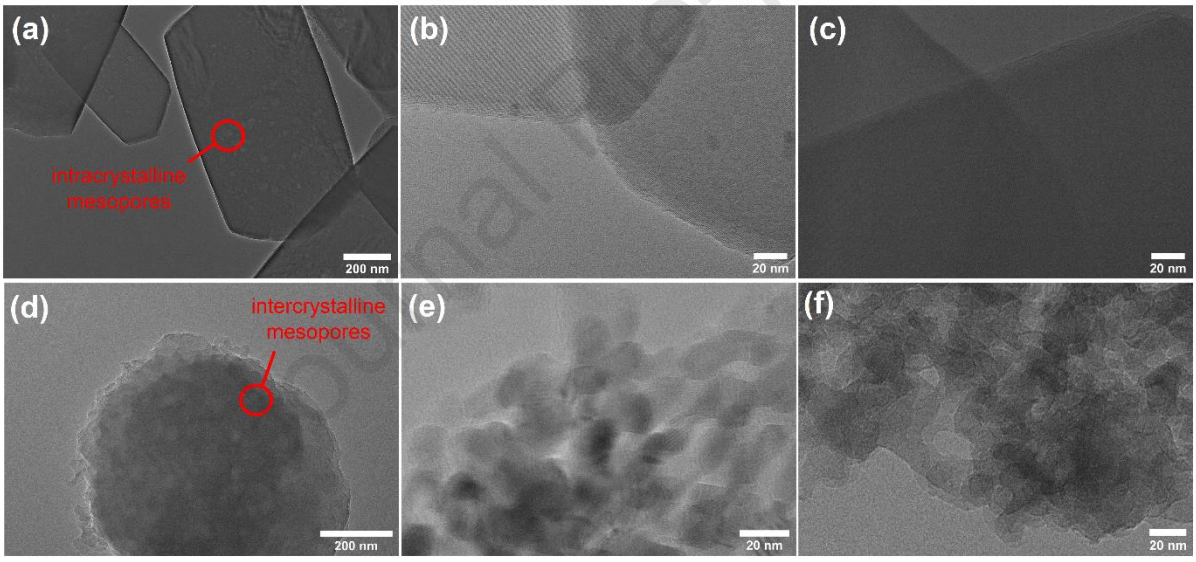

Fig. 5. TEM images of (a) ZHT, (b) Co_3O_4/ZHT2.5, (c) Co_3O_4/ZHT5, (d) ZLT, (e) Co_3O_4/ZLT2.5, and (f) Co_3O_4/ZLT5 catalyst.

The strength and quantity of acid sites on the catalyst surface were studied using NH_3-TPD. As seen in Fig. 6, two distinctive NH_3 desorption peaks were observed for all catalysts at temperatures between 100–300 °C and 300–550 °C. These peaks corresponded to the NH_3 material adsorbed on the weak acid sites and strong acid sites, respectively [57]. Strong acid sites are often introduced by the framework Al, whereas weak acid sites are assumed to be caused by NH_3 adsorption on Si–OH in structural defects [58]. Both the weak and strong acid peaks of Co_3O_4/ZHT (187 and 422 °C) remain unchanged upon the incorporation of Co into

ZHT. In contrast, the Co_3O_4/ZLT peaks of both weak and strong acid sites shifted toward low temperatures (244 and 472 °C for ZLT; 177 and 320 °C for Co_3O_4/ZLT5)

Based on quantitative analysis, ZHT contains more total acidic sites than ZLT, as seen in Table 3. This suggests that ZHT has a higher framework Al content [59], which is supported by the XRF data, which reveal that the Si/Al ratio of ZHT (59) is higher than that of ZLT (74). Moreover, the acidity of ZHT and ZLT decreased as a result of the introduction of Co species into ZSM-5, which is attributed to the exchanges of the Co species with acid protons of Si–O(H)–Al [60]. The findings correspond with XRD data, which demonstrate that the incorporation of Co species reduced the crystallinity of ZSM-5 (Fig. 2) [61].

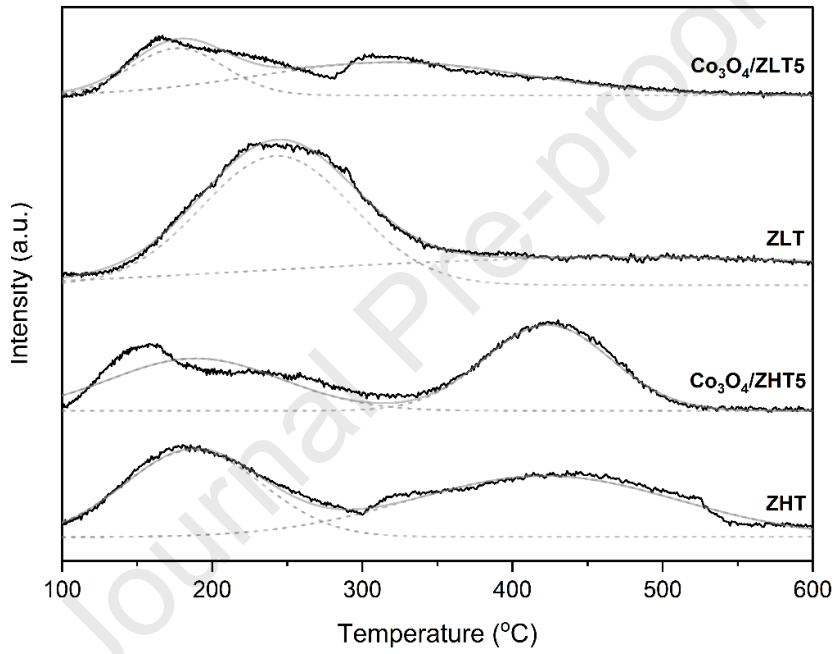

Fig. 6. NH_3-TPD curves of hierarchical ZSM-5 and Co_3O_4/ZSM-5.

Table 3. Analysis of NH_3-TPD data of hierarchical ZSM-5 and Co_3O_4/ZSM-5

Catalyst	**Peak temperature of desorption (°C)**		**Acidic sites**		
	First peak	**Second peak**	**Weak acidic sites [mmol/g]**	**Strong acidic sites [mmol/g]**	**Total acidic sites [mmol/g]**
ZHT	187	422	0.1901	0.2598	0.4499
Co_3O_4/ZHT5	187	422	0.1121	0.1359	0.2480
ZLT	244	472	0.1449	0.1839	0.3288
Co_3O_4/ZLT5	177	320	0.0653	0.1337	0.1990

3.2. Catalytic Tests

Catalytic tests of the as-modified Co_3O_4/ZHT and Co_3O_4/ZLT catalysts were investigated. Methane partial oxidation reactions were carried out in a batch reactor using methane (CH_4) and N_2 (with O_2 0.5%) gas as feedstock with a ratio of 0.75:2.0 bars. Reactions were performed at 150 °C (taken as the optimum temperature based on the work of our group and others) for a variety of time time intervals 30, 60, 90, and 150 min [62–64]. Catalysts were activated at 550 °C for 1 h prior to reactions while the degassing process was carried out using 2 bars of N_2 gas for 10 mins.

Methane could undergo an oxidation reaction to become methanol (CH_3OH), formaldehyde (CH_2O), formic acid (HCOOH) or be completely oxidized into carbon dioxide (CO_2) according to Eq. 5 [65]:

$$CH_4 \rightarrow CH_3OH \rightarrow CH_2O \rightarrow HCOOH \rightarrow CO_2 \quad (5)$$

Fig. 7 presents the temperature relationship of the methane conversion and product yield over the Co_3O_4/ZHT and Co_3O_4/ZLT catalysts. The methane conversion of low-loaded Co_3O_4/ZHT catalyst decreased up to 60 min and increased after 60 min reaction time. The decrease in methane conversion with reaction time may be caused either by a lack of product being recovered from the catalysts or by undiscovered gas products. During the reaction time range of 30–150 min, the methane oxidation reaction catalyzed by Co_3O_4/ZHT catalysts yielded methanol and formaldehyde as the main products. Co_3O_4/ZHT5 produced the highest yield of methanol at 30 min (74.07%); however, the product yield fell after 30 min and methanol was further oxidized into formaldehyde at prolonged reaction time. On the other hand, Co_3O_4/ZHT2.5 exhibits lower yields of methanol at 30 min with the value of 14.35%. Co_3O_4/ZHT2.5 demonstrated the greatest total yield of products in the reaction time of 90 min, with a value of 94.93% (36.02% methanol and 58.91% formaldehyde). However, Co_3O_4/ZHT2.5 shows an increase in the product yield as the reaction time increased. These findings indicate a better catalytic lifetime of Co_3O_4/ZHT2.5 than Co_3O_4/ZHT5 that the product yield decreased after 30 min of reaction time, which may be due to coke deposition in the porous active sites [66].

The methane conversion catalyed by Co_3O_4/ZLT catalysts did not exhibit a similar trend to Co_3O_4/ZHT and instead produced formaldehyde as the main product with a smaller amount of methanol. Furthermore, a small trace of formic acid was found at a reaction time of 120 min. While the results for the product yield of Co_3O_4/ZLT2.5 and Co_3O_4/ZLT5 are comparable, they

differ in that Co_3O_4/ZLT2.5 managed to preserve a higher overall yield of product (13.81%) than Co_3O_4/ZLT5 (4.56%).

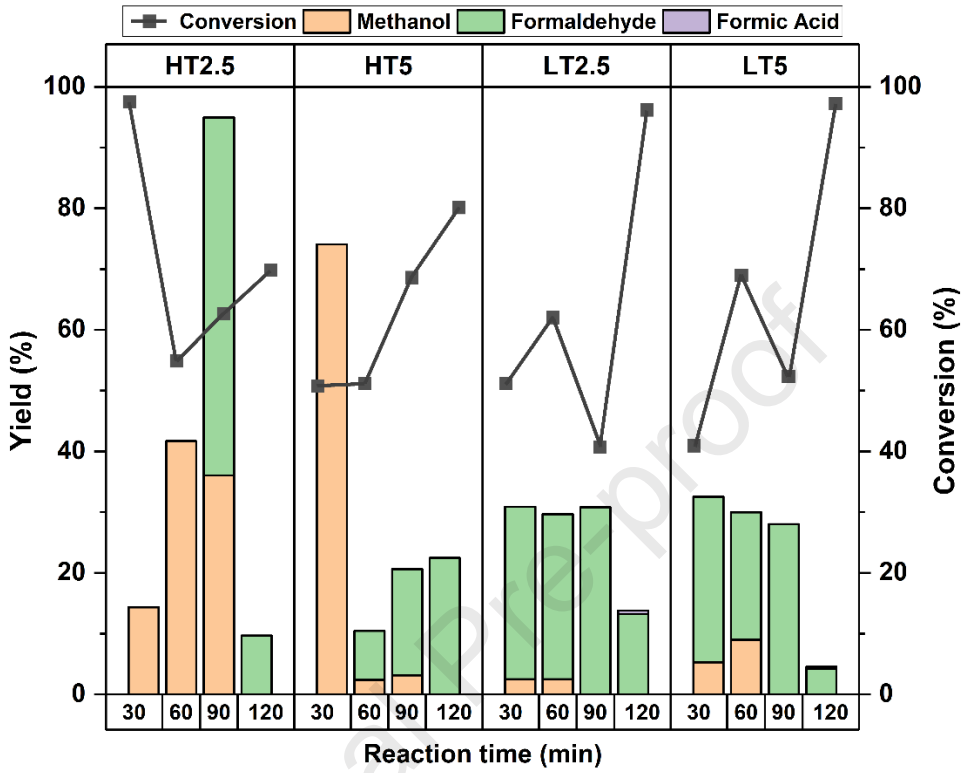

Fig. 7. Catalytic activity in methane partial oxidation of Co_3O_4/ZHT and Co_3O_4/ZLT in terms of products yield and CH_4 conversion as a function of reaction time.

Based on these results, it can be concluded that the optimum reaction time of methane partial oxidation is 90 min, as the yield of products tends to decrease with a prolonged time. Furthermore, Co_3O_4/ZHT and Co_3O_4/ZHT with Co loading 2.5% exhibit better catalytic activity in comparison to higher Co loading. This could be related to metal active sites dispersion into the surface of ZHT and ZLT. These findings also denoted that Co_3O_4 particle size had little or no impact on the methane partial oxidation reaction. Therefore, characterization of the catalysts using XPS and H_2-TPR to further integrate the nature of cobalt oxide species in the catalysts was explored.

The results of methane partial oxidation are consistent with the theoretical value, according to which methane could oxidize into methanol, formaldehyde, and formic acid, and completely oxidize into carbon dioxide. As a result of catalytic tests with a variation of reaction time, Fig. S1 presents a feasible mechanism of methane partial oxidation that modifies the mechanism described by Yumura *et al.* and Krisnandi *et al.* [64,65]. Without the addition of external

oxygen sources, the synthesis of oxygenated products in a batch system could occur by utilizing the free surface-oxygen molecule (O^{2-}) from cobalt oxide molecules by the oxygen vacancy mechanism, as shown in the Fig. S1.

3.3. Extended Characterization: Cobalt Oxide Species

The earlier XRD results on the Co-oxide modification of both ZHT and ZLT show that only a single Co phase of Co_3O_4 existed on the surface of both zeolites. However, despite having apparently similar active sites, and similar cobalt loading values, the Co_3O_4/ZHT and Co_3O_4/ZLT catalysts exhibit different activity for methane partial oxidation. This suggests that Co_3O_4 active sites behave differently due to different environments of hierarchical ZSM-5 with different mesopore configurations of intra- and inter-crystalline mesopores. Therefore, XPS characterization was carried out to understand the state of metal species deposited on the surface of hierarchical ZSM-5 zeolite. Co_3O_4 is the expected form of cobalt oxide based on XRD results and consists of two types of cobalt ion species: Co^{3+} and Co^{2+} with an ideal ratio of 1:2 [67]. The XPS spectra of Co 2p (Fig. 8a) exhibits peaks at Binding Energy (BE) of 777.5–779.5 eV and 793.0–795.0 eV representing Co $2p_{1/2}$ and Co $2p_{3/2}$, respectively [68]. The value of BE split Δ(Co $2p_{1/2}$–Co $2p_{3/2}$) can be related to the cobalt species in the sample specifically Δ(Co $2p_{1/2}$–Co $2p_{3/2}$) = 15.0 eV; 15.7–16.0 eV; or 15.1–15.3 eV representing spin-orbital coupling of Co^{3+} in Co_2O_3, Co^{2+} in CoO, and a mixed valence of Co^{2+} and Co^{3+} in Co_3O_4, respectively [21]. Fig. 8a of modified ZHT and ZLT samples show differences in BE split value of ZHT and ZLT about 15.2 and 15.9–16.0, respectively. These results indicated that the surface cobalt oxide species in ZHT consist of typical Co^{2+} and Co^{3+} mixed species of Co_3O_4, whereas Co^{2+} is the predominant cobalt species in ZLT [69].

Moreover, O 1s spectra (Fig. 8b) of all Co_3O_4-modified catalysts exhibit peaks at BE 530.0–532.0 eV which can be deconvoluted into three oxygen species. The peak at BE 529.5–530.0 eV is indicative of typical surface lattice oxygens (O^{2-}) denoted as O_α. The peak at 531.0–532.0 eV indicates adsorbed oxygen on the surface, denoted as O_β, which plays an important role as an active species in the oxidation reaction [70]. The peak at 533.0–533.5 eV indicates hydroxyl species or water molecules adsorbed on the surface and is denoted as O_γ [71]. Quantitative analysis on the O_β ratio toward total oxygen species (Table 4) suggested the increment of O_β species in the order of Co_3O_4/ZLT5 < Co_3O_4/ZHT5 < Co_3O_4/ZHT2.5 < Co_3O_4/ZLT2.5, with Co_3O_4/ZLT2.5 as the catalyst with the most active surface oxygen species. This result justifies the catalytic tests on Co_3O_4/ZLT which shows selectivity towards

formaldehyde due to its higher surface-adsorbed oxygen value as reflected by $O_\beta/(O_\alpha+O_\beta+O_\gamma)$ value of XPS results.

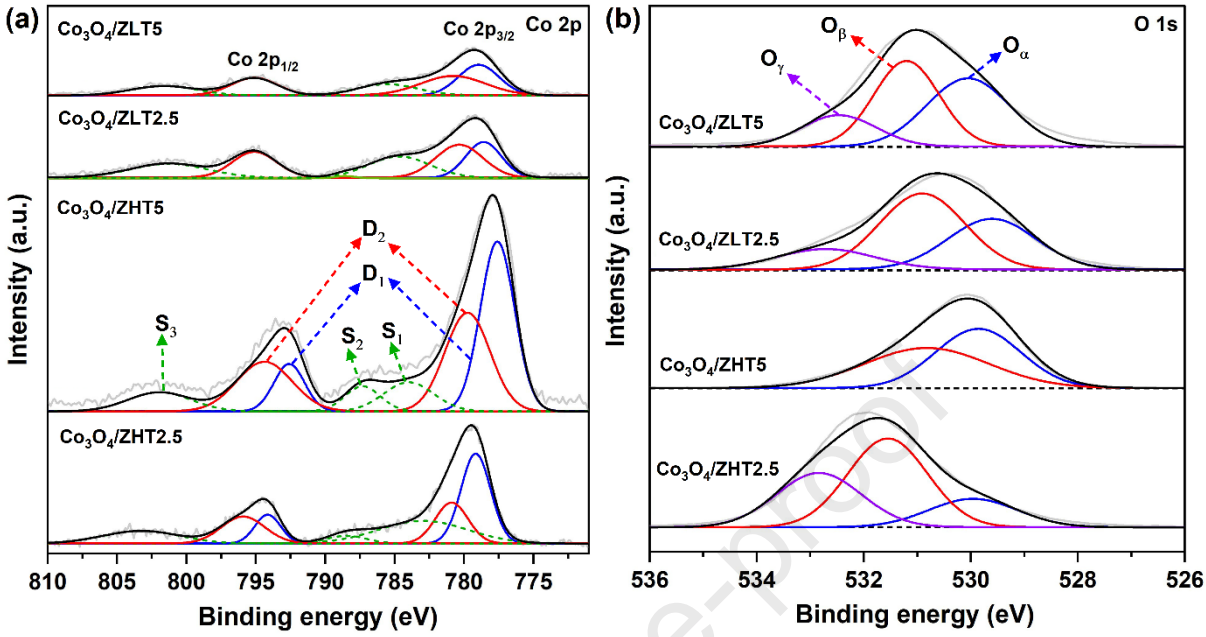

Fig. 8. XPS spectra of hierarchical ZSM-5 catalysts in the range of (a) Co 2p and (b) O 1s.

Table 4. The binding energy and surface content of ZSM-5 catalysts.

Catalyst	Binding energy (eV)	Surface content		
	Δ(Co $2p_{1/2}$–Co $2p_{3/2}$)[a]	Co^{3+}/Co^{2+}	$Co^{3+}/(Co^{3+}+Co^{2+})$ (%)	$O_\beta/(O_\alpha+O_\beta+O_\gamma)$[b] (%)
Co_3O_4/ZHT2.5	15.2 (779.3 – 794.5)	1.4	58.6	49.9
Co_3O_4/ZHT5	15.2 (777.9 – 793.1)	1.0	50.2	49.7
Co_3O_4/ZLT2.5	16.0 (779.1 – 795.1)	0.5	32.4	50.4
Co_3O_4/ZLT5	15.9 (779.1 – 795.0)	0.6	38.1	41.1

[a] The difference (Δ) between Co $2p_{3/2}$ and Co $2p_{1/2}$ binding energy.
[b] O_α is the surface lattice oxygen; O_β is the surface-adsorbed oxygen; O_γ is the surface hydroxyl species (OH).

H_2-TPR characterization was carried out to confirm XPS and catalytic results by analysing the reduction behaviour of cobalt species on the as-modified hierarchical ZHT and ZLT with 5% Co_3O_4 percent loading (Fig. 9). Theoretically, Co_3O_4 reduction proceed in two steps: $Co_3O_4 \rightarrow CoO \rightarrow Co^0$ with every step reflected as a peak on the H_2-TPR profile and could be divided into three reduction regions: region I (< 400 °C) representing the reduction of extra-framework Co_3O_4 to CoO (Co^{3+} bulky species to Co^{2+}), region II (400–700 °C) representing the reduction of intra-framework $(CoO_x)_n$ oligomers Co^{2+} to Co^0 and region III (700–900 °C) representing

the reduction of extra-framework phyllosilicate Co(II). Furthermore, isolated Co^{2+} species could also reduce at high temperatures (> 900 °C) [22,72].

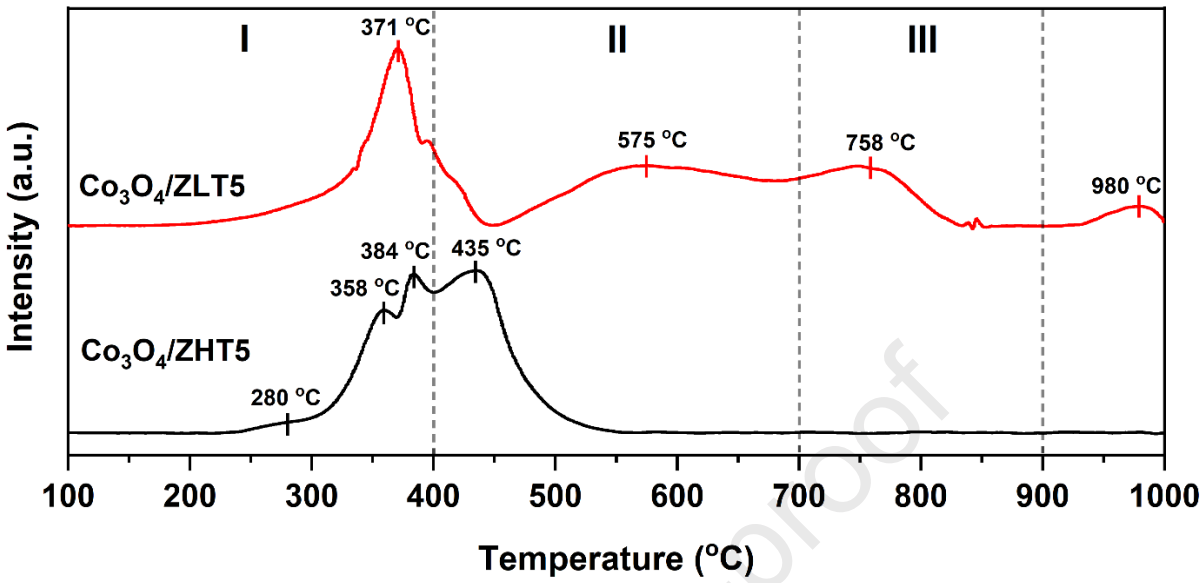

Fig. 9. H_2-TPR profile of Co-oxide modified hierarchical ZSM-5 catalyst.

Table 5. H_2-TPR analysis of ZSM-5 catalysts.

Catalyst	Peak temperature (°C)			H_2 uptake (%)			
	I	II	III	Co^{x+} in Co_3O_4	Co^{2+} in CoO	$CoSiO_4$	Isolated Co^{2+}
Co_3O_4/ZHT5	280; 358; 384	435	-	46.8	53.2	-	-
Co_3O_4/ZLT5	371	575	758	40.3	34.4	21.8	3.5

The H_2-TPR profile of Co_3O_4/ZHT5 and Co_3O_4/ZLT5 in Fig. 9 showed a quite different reduction behaviour which was later quantified in Table 5. The Co_3O_4/ZHT5 sample was observed to exhibit four main peaks in region I and II indicating that Co_3O_4 was completely reduced. Meanwhile, Co_3O_4/ZLT5 exhibits four main peaks in the region I, II, and III, with an additional isolated Co^{2+} peak at 980 °C. These results indicated that Co_3O_4 deposited on ZLT contains phyllosilicate Co(II) when Co species reacts with the zeolite surface leading to the creation of hard-to-reduce silicate layer deposits that are tightly bonded [73]. Furthermore, Co^{2+} peaks present in Co_3O_4/ZLT5 indicate the predominance of Co^{2+} species on ZLT, which is in good agreement with XPS results. Good dispersion of Co oxide particles on the ZLT which is shown by SEM and TEM directs to the strong interaction of Co oxide on the ZLT support and hinders the reduction of Co(II) to Co^0 [28]. Therefore, it is known that porosity and mesopores configuration influence the particle size of Co_3O_4, which leads to the conclusion

that mesopores configuration of intra- and inter-crystalline play an important role in affecting the predominant Co species and reduction feature of Co oxide on hierarchical ZSM-5.

4. Conclusions

Hierarchical ZSM-5 with two types of mesopore configuration (intracrystalline and inter-crystalline mesopores) were synthesized and employed as a catalyst for methane partial oxidation reaction. Mesopore configuration of hierarchical ZSM-5 affected the physicochemical properties and character of impregnated Co_3O_4. Hierarchical ZSM-5 with inter-crystalline mesopores presented better dispersion of Co_3O_4 dominated by Co(II) species, while hierarchical ZSM-5 with intracrystalline mesopores type showed smaller mesopore size with a fair amount of Co(III) and Co(II) species. Furthermore, hierarchical ZSM-5 with inter-crystalline mesopores demonstrated strong oxidation activity as reflected by the formation of formaldehyde in the brief reaction time. ZSM-5 cobalt loading of 2.5% presented a superior catalytic performance in terms of yield, conversion, and lifetime compared to higher cobalt loading.

Supporting Information

Detailed information on the methane partial oxidation reaction mechanism is provided in supporting information.

Author Contributions

Irena Khatrin: Writing – original draft, Writing – review & editing, Investigation, Formal analysis, Methodology, Data curation, Validation; Iman Abdullah: Conceptualization, Methodology, Supervision; Alan McCue: Methodology, Formal analysis, Writing – review & editing; Yuni K. Krisnandi: Conceptualization, Writing – review & editing, Formal analysis, Funding acquisition, Supervision.

Acknowledgment

This work was supported by Universitas Indonesia through Hibah Publikasi Terindeks Internasional (PUTI) Q2 Research Grant No. NKB-671/UN2.RST/HKP.05.00/2022 and

Indonesian Ministry of Research, Technology and Higher Education (Menristekdikti) through Pendidikan Magister menuju Doktor untuk Sarjana Unggul (PMDSU) Research Grant No. NKB-895/UN2.RST/HKP.05.00/2023.

References

[1] S. Dong, H. Li, I.K. Bloede, A.J. Al Abdulghani, E.A. Lebrón-Rodríguez, G.W. Huber, I. Hermans, Catalytic conversion of model compounds of plastic pyrolysis oil over ZSM-5, Appl Catal B. 324 (2023) 122219. https://doi.org/10.1016/J.APCATB.2022.122219.

[2] G. Qi, T.E. Davies, A. Nasrallah, M.A. Sainna, A.G.R. Howe, R.J. Lewis, M. Quesne, C.R.A. Catlow, D.J. Willock, Q. He, D. Bethell, M.J. Howard, B.A. Murrer, B. Harrison, C.J. Kiely, X. Zhao, F. Deng, J. Xu, G.J. Hutchings, Au-ZSM-5 catalyses the selective oxidation of CH4 to CH3OH and CH3COOH using O2, Nature Catalysis 2022 5:1. 5 (2022) 45–54. https://doi.org/10.1038/s41929-021-00725-8.

[3] A. López-Martín, M.F. Sini, M.G. Cutrufello, A. Caballero, G. Colón, Characterization of Re-Mo/ZSM-5 catalysts: How Re improves the performance of Mo in the methane dehydroaromatization reaction, Appl Catal B. 304 (2022) 120960. https://doi.org/10.1016/J.APCATB.2021.120960.

[4] H.O. Mohamed, R.K. Parsapur, I. Hita, J.L. Cerrillo, A. Ramírez, K.W. Huang, J. Gascon, P. Castaño, Stable and reusable hierarchical ZSM-5 zeolite with superior performance for olefin oligomerization when partially coked, Appl Catal B. 316 (2022) 121582. https://doi.org/10.1016/J.APCATB.2022.121582.

[5] A. Bonilla, D. Baudouin, J. Pérez-Ramírez, Desilication of ferrierite zeolite for porosity generation and improved effectiveness in polyethylene pyrolysis, J Catal. 265 (2009) 170–180. https://doi.org/10.1016/J.JCAT.2009.04.022.

[6] R. Bai, Y. Song, Y. Li, J. Yu, Creating Hierarchical Pores in Zeolite Catalysts, Trends Chem. 1 (2019) 601–611. https://doi.org/10.1016/j.trechm.2019.05.010.

[7] Y. Wang, J. Yu, J. Qiao, Y. Sun, W. Jin, H. Zhang, J. Ma, Effect of mesoporous ZSM-5 morphology on the catalytic performance of cobalt catalyst for Fischer-Tropsch synthesis, Journal of the Energy Institute. 93 (2020) 1187–1194. https://doi.org/10.1016/J.JOEI.2019.11.002.

[8] K. Möller, T. Bein, Mesoporosity – a new dimension for zeolites, Chem Soc Rev. 42 (2013) 3689–3707. https://doi.org/10.1039/c3cs35488a.

[9] J. Pérez-Ramírez, C.H. Christensen, K. Egeblad, C.H. Christensen, J.C. Groen, Hierarchical zeolites: enhanced utilisation of microporous crystals in catalysis by advances in materials design, Chem Soc Rev. 37 (2008) 2530–2542. https://doi.org/10.1039/B809030K.

[10] I. Khatrin, R.H. Kusuma, G.T.M. Kadja, Y.K. Krisnandi, Significance of ZSM-5 hierarchical structure on catalytic cracking: Intra- vs inter-crystalline mesoporosity, Inorg Chem Commun. 149 (2023) 110447. https://doi.org/10.1016/J.INOCHE.2023.110447.

[11] V.D.B.C. Dasireddy, B. Likozar, Direct methanol production from mixed methane/H2O/N2O feedstocks over Cu–Fe/Al2O3 catalysts, Fuel. 301 (2021). https://doi.org/10.1016/j.fuel.2021.121084.

[12] H. Zuo, Q. Xin, V. Meynen, E. Klemm, Sensitivity of the selective oxidation of methane over Fe/ZSM-5 zeolites in a micro fixed-bed reactor for the catalyst preparation method, Appl Catal A Gen. 566 (2018) 96–103. https://doi.org/10.1016/j.apcata.2018.08.022.

[13] M. Ravi, M. Ranocchiari, J.A. van Bokhoven, The Direct Catalytic Oxidation of Methane to Methanol—A Critical Assessment, Angewandte Chemie International Edition. 56 (2017) 16464–16483. https://doi.org/https://doi.org/10.1002/anie.201702550.

[14] S. Wang, H. Zhang, M. Wang, X. Liu, S. Shang, Z. Wang, C. Zhang, Micro-meso hierarchical ZSM-5 zeolite supported RuOx nanoparticles for activity enhancement of catalytic vinyl chloride oxidation, Appl Surf Sci. 606 (2022) 154906. https://doi.org/10.1016/J.APSUSC.2022.154906.

[15] T. Dong, W. Liu, M. Ma, H. Peng, S. Yang, J. Tao, C. He, L. Wang, P. Wu, T. An, Hierarchical zeolite enveloping Pd-CeO2 nanowires: An efficient adsorption/catalysis bifunctional catalyst for low temperature propane total degradation, Chemical Engineering Journal. 393 (2020) 124717. https://doi.org/10.1016/J.CEJ.2020.124717.

[16] T. Barakat, J.C. Rooke, H.L. Tidahy, M. Hosseini, R. Cousin, J.F. Lamonier, J.M. Giraudon, G. De Weireld, B.L. Su, S. Siffert, Noble-Metal-Based Catalysts Supported

on Zeolites and Macro-Mesoporous Metal Oxide Supports for the Total Oxidation of Volatile Organic Compounds, ChemSusChem. 4 (2011) 1420–1430. https://doi.org/10.1002/CSSC.201100282.

[17] J. Han, J. Cho, J.C. Kim, R. Ryoo, Confinement of Supported Metal Catalysts at High Loading in the Mesopore Network of Hierarchical Zeolites, with Access via the Microporous Windows, ACS Catal. 8 (2018) 876–879. https://doi.org/10.1021/ACSCATAL.7B04183/SUPPL_FILE/CS7B04183_SI_001.PDF.

[18] G.T.M. Kadja, R.R. Mukti, Z. Liu, M. Rilyanti, Ismunandar, I.N. Marsih, M. Ogura, T. Wakihara, T. Okubo, Mesoporogen-free synthesis of hierarchically porous ZSM-5 below 100°C, Microporous and Mesoporous Materials. 226 (2016) 344–352. https://doi.org/10.1016/j.micromeso.2016.02.007.

[19] C. Liu, W. Gu, D. Kong, H. Guo, The significant effects of the alkali-metal cations on ZSM-5 zeolite synthesis: From mechanism to morphology, Microporous and Mesoporous Materials. 183 (2014) 30–36. https://doi.org/10.1016/J.MICROMESO.2013.08.037.

[20] S. Sang, F. Chang, Z. Liu, C. He, Y. He, L. Xu, Difference of ZSM-5 zeolites synthesized with various templates, Catal Today. 93–95 (2004) 729–734. https://doi.org/10.1016/J.CATTOD.2004.06.091.

[21] C. Zhang, Y. Wang, G. Li, L. Chen, Q. Zhang, D. Wang, X. Li, Z. Wang, Tuning smaller Co3O4 nanoparticles onto HZSM-5 zeolite via complexing agents for boosting toluene oxidation performance, Appl Surf Sci. 532 (2020) 147320. https://doi.org/10.1016/J.APSUSC.2020.147320.

[22] Z. Zhu, G. Lu, Z. Zhang, Y. Guo, Y. Guo, Y. Wang, Highly active and stable Co3O4/ZSM-5 catalyst for propane oxidation: Effect of the preparation method, ACS Catal. 3 (2013) 1154–1164. https://doi.org/10.1021/CS400068V/ASSET/IMAGES/MEDIUM/CS-2013-00068V_0016.GIF.

[23] M.M.J. Treacy, J.B. Higgins, Collection of Simulated XRD Powder Patterns for Zeolites, 2007. https://doi.org/10.1016/B978-044453067-7/50604-3.

[24] X. Fei, S. Cao, W. Ouyang, Y. Wen, H. Wang, Z. Wu, A convenient synthesis of core-shell Co3O4@ZSM-5 catalysts for the total oxidation of dichloromethane (CH2Cl2), Chemical Engineering Journal. 387 (2020) 123411. https://doi.org/10.1016/J.CEJ.2019.123411.

[25] W. Ma, D. Ye, H. Wang, Experimental Study on the Elemental Mercury Removal Performance and Regeneration Ability of CoOx–FeOx-Modified ZSM-5 Adsorbents, Applied Sciences (Switzerland). 12 (2022) 3769. https://doi.org/10.3390/APP12083769/S1.

[26] H. Schneider, L.K. Schindel, L.B. Gomes, I.C. Tessaro, N.R. Marcilio, Template-free ZSM-5 membrane preparation on alumina support by secondary hydrothermal synthesis, Current Research in Green and Sustainable Chemistry. 4 (2021) 100049. https://doi.org/10.1016/J.CRGSC.2020.100049.

[27] T. Gille, M. Seifert, M.S. Marschall, S. Bredow, T. Schneider, O. Busse, W. Reschetilowski, J.J. Weigand, Conversion of Oxygenates on H-ZSM-5 Zeolites—Effects of Feed Structure and Si/Al Ratio on the Product Quality, Catalysts 2021, Vol. 11, Page 432. 11 (2021) 432. https://doi.org/10.3390/CATAL11040432.

[28] J.E. Min, S. Kim, G. Kwak, Y.T. Kim, S.J. Han, Y. Lee, K.W. Jun, S.K. Kim, Role of mesopores in Co/ZSM-5 for the direct synthesis of liquid fuel by Fischer–Tropsch synthesis, Catal Sci Technol. 8 (2018) 6346–6359. https://doi.org/10.1039/C8CY01931B.

[29] C.F. Liu, L.C. He, X.F. Wang, J. Chen, J.Q. Lu, M.F. Luo, Tailoring Co3O4 active species to promote propane combustion over Co3O4/ZSM-5 catalyst, Molecular Catalysis. 524 (2022) 112297. https://doi.org/10.1016/J.MCAT.2022.112297.

[30] W. Ma, D. Ye, H. Wang, Experimental Study on the Elemental Mercury Removal Performance and Regeneration Ability of CoOx–FeOx-Modified ZSM-5 Adsorbents, Applied Sciences (Switzerland). 12 (2022) 3769. https://doi.org/10.3390/APP12083769/S1.

[31] M. Zabihi, N. Babajani, Modeling, optimization and experimental studies of supported nano-bimetallic catalyst for simultaneous total conversion of toluene and cyclohexane in air using a hybrid intelligent algorithm, RSC Adv. 8 (2018) 17346–17356. https://doi.org/10.1039/C8RA01504J.

[32] A. Sridhar, M. Rahman, A. Infantes-Molina, B.J. Wylie, C.G. Borcik, S.J. Khatib, Bimetallic Mo-Co/ZSM-5 and Mo-Ni/ZSM-5 catalysts for methane dehydroaromatization: A study of the effect of pretreatment and metal loadings on the catalytic behavior, Appl Catal A Gen. 589 (2020) 117247. https://doi.org/10.1016/J.APCATA.2019.117247.

[33] Y. Xu, Q. Wang, B.A. Yoza, Q.X. Li, Y. Kou, Y. Tang, H. Ye, Y. Li, C. Chen, Catalytic ozonation of recalcitrant organic chemicals in water using vanadium oxides loaded ZSM-5 zeolites, Front Chem. 7 (2019) 384. https://doi.org/10.3389/FCHEM.2019.00384/BIBTEX.

[34] I. Othman Ali, A.M. Hassan, S.M. Shaaban, K.S. Soliman, Synthesis and characterization of ZSM-5 zeolite from rice husk ash and their adsorption of Pb2+ onto unmodified and surfactant-modified zeolite, Sep Purif Technol. 83 (2011) 38–44. https://doi.org/10.1016/J.SEPPUR.2011.08.034.

[35] G.T. Kokotailo, S.L. Lawton, D.H. Olson, W.M. Meier, Structure of synthetic zeolite ZSM-5, Nature 1978 272:5652. 272 (1978) 437–438. https://doi.org/10.1038/272437a0.

[36] X. Guan, C. Duan, H. Wang, B. Lu, J. Zhao, Q. Cai, Tuneable oxidation of styrene to benzaldehyde and benzoic acid over Co/ZSM-5, New Journal of Chemistry. 45 (2021) 18192–18201. https://doi.org/10.1039/D1NJ03145G.

[37] R. Sabarish, G. Unnikrishnan, Synthesis, characterization and catalytic activity of hierarchical ZSM-5 templated by carboxymethyl cellulose, Powder Technol. 320 (2017) 412–419. https://doi.org/10.1016/J.POWTEC.2017.07.041.

[38] A. Kostyniuk, D. Key, M. Mdleleni, 1-hexene isomerization over bimetallic M-Mo-ZSM-5 (M: Fe, Co, Ni) zeolite catalysts: Effects of transition metals addition on the catalytic performance, Journal of the Energy Institute. 93 (2020) 552–564. https://doi.org/10.1016/J.JOEI.2019.06.009.

[39] D.P. Serrano, T.J. Pinnavaia, J. Aguado, J.M. Escola, A. Peral, L. Villalba, Hierarchical ZSM-5 zeolites synthesized by silanization of protozeolitic units: Mediating the mesoporosity contribution by changing the organosilane type, Catal Today. 227 (2014) 15–25. https://doi.org/10.1016/J.CATTOD.2013.10.052.

[40] W. Luo, X. Yang, Z. Wang, W. Huang, J. Chen, W. Jiang, L. Wang, X. Cheng, Y. Deng, D. Zhao, Synthesis of ZSM-5 aggregates made of zeolite nanocrystals through a simple solvent-free method, Microporous and Mesoporous Materials. 243 (2017) 112–118. https://doi.org/10.1016/J.MICROMESO.2017.01.040.

[41] G. Song, W. Chen, P. Dang, S. Yang, Y. Zhang, Y. Wang, R. Xiao, R. Ma, F. Li, Synthesis and Characterization of Hierarchical ZSM-5 Zeolites with Outstanding Mesoporosity and Excellent Catalytic Properties, Nanoscale Res Lett. 13 (2018) 1–13. https://doi.org/10.1186/S11671-018-2779-8/FIGURES/11.

[42] C. Fan, Z. Wu, Z. Li, Z. Qin, H. Zhu, M. Dong, J. Wang, W. Fan, Controllable preparation of ultrafine Co3O4 nanoparticles on H-ZSM-5 with superior catalytic performance in lean methane combustion, Fuel. 334 (2023) 126815. https://doi.org/10.1016/J.FUEL.2022.126815.

[43] A. Kumar, R. Prasad, Y.C. Sharma, Ethanol steam reforming study over ZSM-5 supported cobalt versus nickel catalyst for renewable hydrogen generation, Chin J Chem Eng. 27 (2019) 677–684. https://doi.org/10.1016/J.CJCHE.2018.03.036.

[44] E. Mohiuddin, M.M. Mdleleni, D. Key, Catalytic cracking of naphtha: The effect of Fe and Cr impregnated ZSM-5 on olefin selectivity, Applied Petrochemical Research 2018 8:2. 8 (2018) 119–129. https://doi.org/10.1007/S13203-018-0200-2.

[45] B. Ba Mohammed, A. Hsini, Y. Abdellaoui, H. Abou Oualid, M. Laabd, M. El Ouardi, A. Ait Addi, K. Yamni, N. Tijani, Fe-ZSM-5 zeolite for efficient removal of basic Fuchsin dye from aqueous solutions: Synthesis, characterization and adsorption process optimization using BBD-RSM modeling, J Environ Chem Eng. 8 (2020) 104419. https://doi.org/10.1016/J.JECE.2020.104419.

[46] K. CHEN, T. ZHANG, X. CHEN, Y. HE, X. LIANG, Model construction of micro-pores in shale: A case study of Silurian Longmaxi Formation shale in Dianqianbei area, SW China, Petroleum Exploration and Development. 45 (2018) 412–421. https://doi.org/10.1016/S1876-3804(18)30046-6.

[47] Y. Gao, B. Zheng, G. Wu, F. Ma, C. Liu, Effect of the Si/Al ratio on the performance of hierarchical ZSM-5 zeolites for methanol aromatization, RSC Adv. 6 (2016) 83581–83588. https://doi.org/10.1039/C6RA17084F.

[48] W. Li, T. Ma, Y. Zhang, Y. Gong, Z. Wu, T. Dou, Facile control of inter-crystalline porosity in the synthesis of size-controlled mesoporous MFI zeolites via in situ conversion of silica gel into zeolite nanocrystals for catalytic cracking, CrystEngComm. 17 (2015) 5680–5689. https://doi.org/10.1039/C5CE00637F.

[49] H. Zhang, Y. Ma, K. Song, Y. Zhang, Y. Tang, Nano-crystallite oriented self-assembled ZSM-5 zeolite and its LDPE cracking properties: Effects of accessibility and strength of acid sites, J Catal. 302 (2013) 115–125. https://doi.org/10.1016/J.JCAT.2013.03.019.

[50] K. Qiao, F. Zhou, Z. Han, J. Fu, H. Ma, G. Wu, Synthesis and physicochemical characterization of hierarchical ZSM-5: Effect of organosilanes on the catalyst properties and performance in the catalytic fast pyrolysis of biomass, Microporous and Mesoporous Materials. 274 (2019) 190–197. https://doi.org/10.1016/J.MICROMESO.2018.07.028.

[51] C. Liu, Y. Chen, Y. Zhao, S. Lyu, L. Wei, X. Li, Y. Zhang, J. Li, Nano-ZSM-5-supported cobalt for the production of liquid fuel in Fischer-Tropsch synthesis: Effect of preparation method and reaction temperature, Fuel. 263 (2020) 116619. https://doi.org/10.1016/J.FUEL.2019.116619.

[52] M. Hamidzadeh, M. Saeidi, S. Komeili, Modified seeding method to produce hierarchical nanocrystalline ZSM-5 zeolite, Mater Today Commun. 25 (2020) 101308. https://doi.org/10.1016/J.MTCOMM.2020.101308.

[53] F. Subhan, S. Aslam, Z. Yan, Z. Liu, U.J. Etim, A. Wadood, R. Ullah, Confinement of mesopores within ZSM-5 and functionalization with Ni NPs for deep desulfurization, Chemical Engineering Journal. 354 (2018) 706–715. https://doi.org/10.1016/J.CEJ.2018.08.059.

[54] L. Yang, Z. Liu, Z. Liu, W. Peng, Y. Liu, C. Liu, Correlation between H-ZSM-5 crystal size and catalytic performance in the methanol-to-aromatics reaction, Chinese Journal of Catalysis. 38 (2017) 683–690. https://doi.org/10.1016/S1872-2067(17)62791-8.

[55] Y. Gu, X. Wang, Z. Qin, S. Mintova, X. Liu, Intra-crystalline mesoporous ZSM-5 zeolite by grinding synthesis method, Microporous and Mesoporous Materials. 306 (2020) 110437. https://doi.org/10.1016/J.MICROMESO.2020.110437.

[56] J. Liu, Z. Wang, P. Jian, R. Jian, Highly selective oxidation of styrene to benzaldehyde over a tailor-made cobalt oxide encapsulated zeolite catalyst, J Colloid Interface Sci. 517 (2018) 144–154. https://doi.org/10.1016/J.JCIS.2018.01.113.

[57] Z. Jiang, D. Chen, W. Deng, L. Guo, Different morphological ZSM-5 zeolites supported Pt catalysts for toluene catalytic combustion, Chemical Physics Impact. 5 (2022) 100134. https://doi.org/10.1016/J.CHPHI.2022.100134.

[58] X. Guan, C. Duan, H. Wang, B. Lu, J. Zhao, Q. Cai, Tuneable oxidation of styrene to benzaldehyde and benzoic acid over Co/ZSM-5, New Journal of Chemistry. 45 (2021) 18192–18201. https://doi.org/10.1039/D1NJ03145G.

[59] H. Wang, P. Gao, S. Li, T. Wang, C. Yang, J. Li, T. Lin, L. Zhong, Y. Sun, Bifunctional catalysts with versatile zeolites enable unprecedented para-xylene productivity for syngas conversion under mild conditions, Chem Catalysis. 2 (2022) 779–796. https://doi.org/10.1016/J.CHECAT.2022.01.014.

[60] L. Wu, Z. Fu, J. Wei, H. Deng, Y. Zhang, Y. Tang, L. Tan, The investigation into the dehydroaromatization of ethane over cobalt-modified ZSM-5 catalyst, Microporous and Mesoporous Materials. 343 (2022) 112159. https://doi.org/10.1016/J.MICROMESO.2022.112159.

[61] Y. Wang, J. Yu, J. Qiao, Y. Sun, W. Jin, H. Zhang, J. Ma, Effect of mesoporous ZSM-5 morphology on the catalytic performance of cobalt catalyst for Fischer-Tropsch synthesis, Journal of the Energy Institute. 93 (2020) 1187–1194. https://doi.org/10.1016/J.JOEI.2019.11.002.

[62] N. V. Beznis, A.N.C. Van Laak, B.M. Weckhuysen, J.H. Bitter, Oxidation of methane to methanol and formaldehyde over Co-ZSM-5 molecular sieves: Tuning the reactivity and selectivity by alkaline and acid treatments of the zeolite ZSM-5 agglomerates, Microporous and Mesoporous Materials. 138 (2011) 176–183. https://doi.org/10.1016/j.micromeso.2010.09.009.

[63] Y.K. Krisnandi, B.A.P. Putra, M. Bahtiar, Zahara, I. Abdullah, R.F. Howe, Partial Oxidation of Methane to Methanol over Heterogeneous Catalyst Co/ZSM-5, Procedia Chem. 14 (2015) 508–515. https://doi.org/10.1016/j.proche.2015.03.068.

[64] Y.K. Krisnandi, D.A. Nurani, D. V. Alfian, U. Sofyani, M. Faisal, I.R. Saragi, A.Z. Pamungkas, A.P. Pratama, The new challenge of partial oxidation of methane over Fe2O3/NaY and Fe3O4/NaY heterogeneous catalysts, Heliyon. 7 (2021). https://doi.org/10.1016/j.heliyon.2021.e08305.

[65] T. Yumura, T. Amenomori, Y. Kagawa, K. Yoshizawa, Mechanism for the Formaldehyde to Formic Acid and the Formic Acid to Carbon Dioxide Conversions Mediated by an Iron-Oxo Species, Journal of Physical Chemistry A. 106 (2002) 621–630. https://doi.org/10.1021/JP0122225.

[66] M. Ghaedi, A. Izadbakhsh, Effects of Ca content on the activity of HZSM-5 nanoparticles in the conversion of methanol to olefins and coke formation, Ranliao Huaxue Xuebao/Journal of Fuel Chemistry and Technology. 49 (2021) 1468–1486. https://doi.org/10.1016/S1872-5813(21)60130-5.

[67] T.R. Paudel, A. Zakutayev, S. Lany, M. D'Avezac, A. Zunger, Doping Rules and Doping Prototypes in A2BO4 Spinel Oxides, Adv Funct Mater. 21 (2011) 4493–4501. https://doi.org/10.1002/ADFM.201101469.

[68] O.B. Ayodele, Influence of oxalate ligand functionalization on Co/ZSM-5 activity in Fischer Tropsch synthesis and hydrodeoxygenation of oleic acid into hydrocarbon fuels, Scientific Reports 2017 7:1. 7 (2017) 1–14. https://doi.org/10.1038/s41598-017-09706-z.

[69] M.I. Shilina, T.N. Rostovshchikova, S.A. Nikolaev, O. V. Udalova, Polynuclear Co-oxo cations in the catalytic oxidation of CO on Co-modified ZSM-5 zeolites, Mater Chem Phys. 223 (2019) 287–298. https://doi.org/10.1016/J.MATCHEMPHYS.2018.11.005.

[70] X. Xu, H. Han, J. Liu, W. Liu, W. Li, X. Wang, Promotional effects of samarium on Co3O4 spinel for CO and CH4 oxidation, Journal of Rare Earths. 32 (2014) 159–169. https://doi.org/10.1016/S1002-0721(14)60046-6.

[71] E. Wu, X. Feng, Y. Zheng, D. Lin, Y. Luo, Y. You, B. Huang, Q. Qian, Q. Chen, Inverse Coprecipitation Directed Porous Core-Shell Mn-Co-O Catalyst for Efficient Low Temperature Propane Oxidation, ACS Sustain Chem Eng. 8 (2020) 5787–5798. https://doi.org/10.1021/ACSSUSCHEMENG.0C01497/SUPPL_FILE/SC0C01497_SI_001.PDF.

[72] N. V. Beznis, B.M. Weckhuysen, J.H. Bitter, Partial oxidation of methane over Co-ZSM-5: Tuning the oxygenate selectivity by altering the preparation route, Catal Letters. 136 (2010) 52–56. https://doi.org/10.1007/S10562-009-0206-6/FIGURES/4.

[73] C. Chupin, A.C. van Veen, M. Konduru, J. Després, C. Mirodatos, Identity and location of active species for NO reduction by CH4 over Co-ZSM-5, J Catal. 241 (2006) 103–114. https://doi.org/10.1016/J.JCAT.2006.04.025.

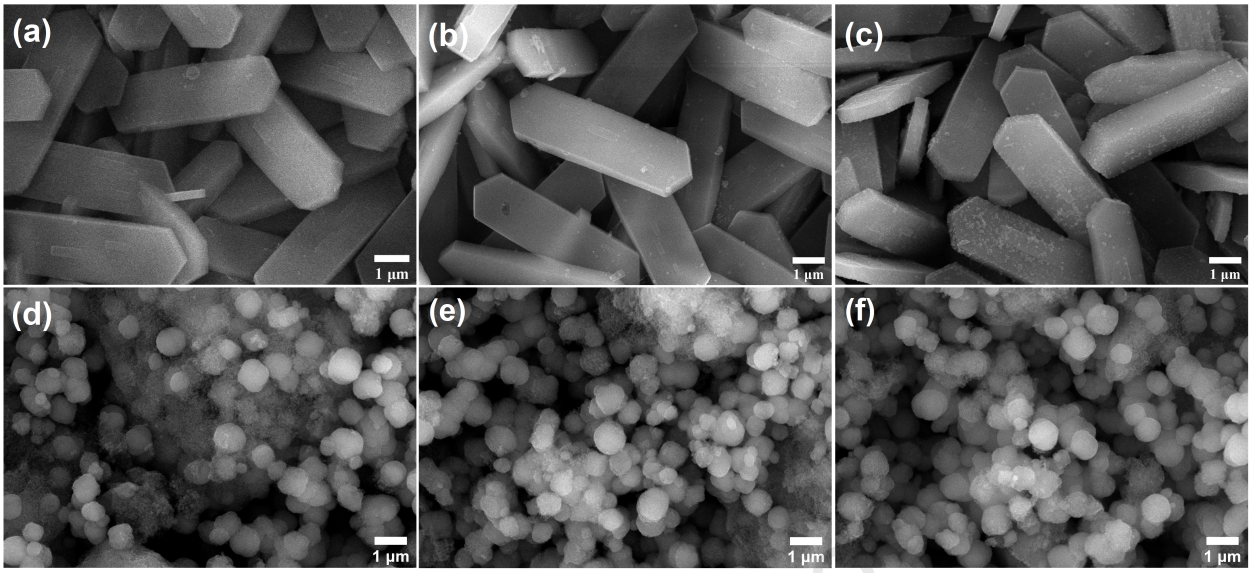

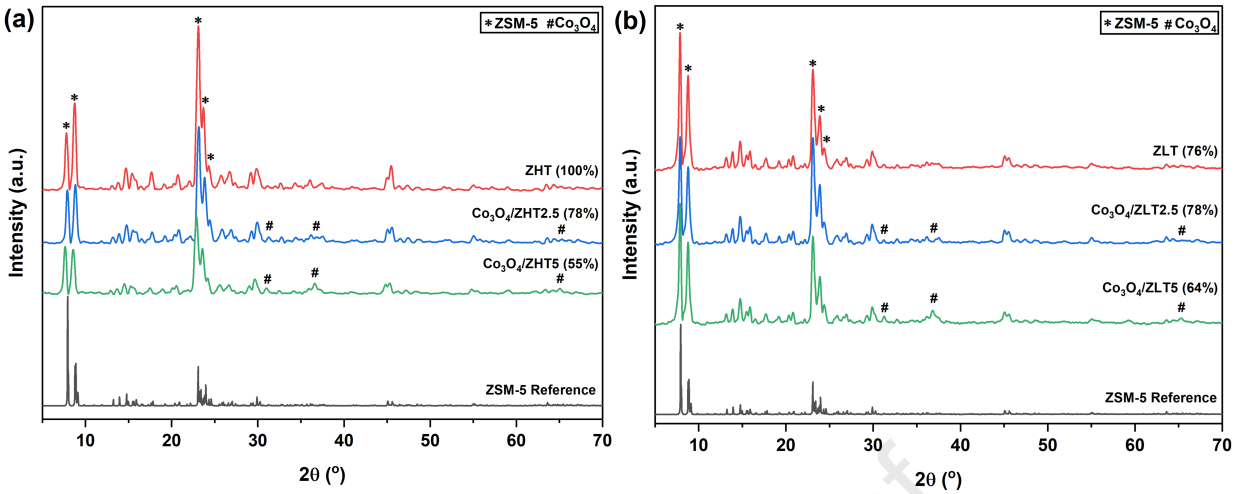

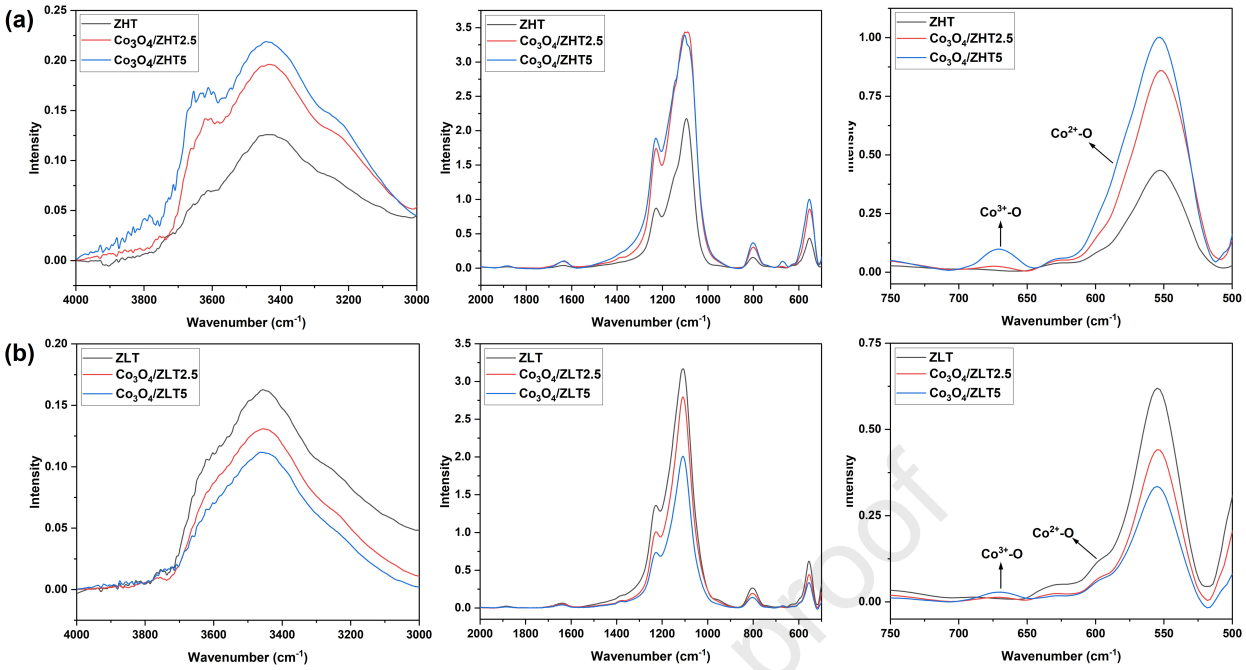

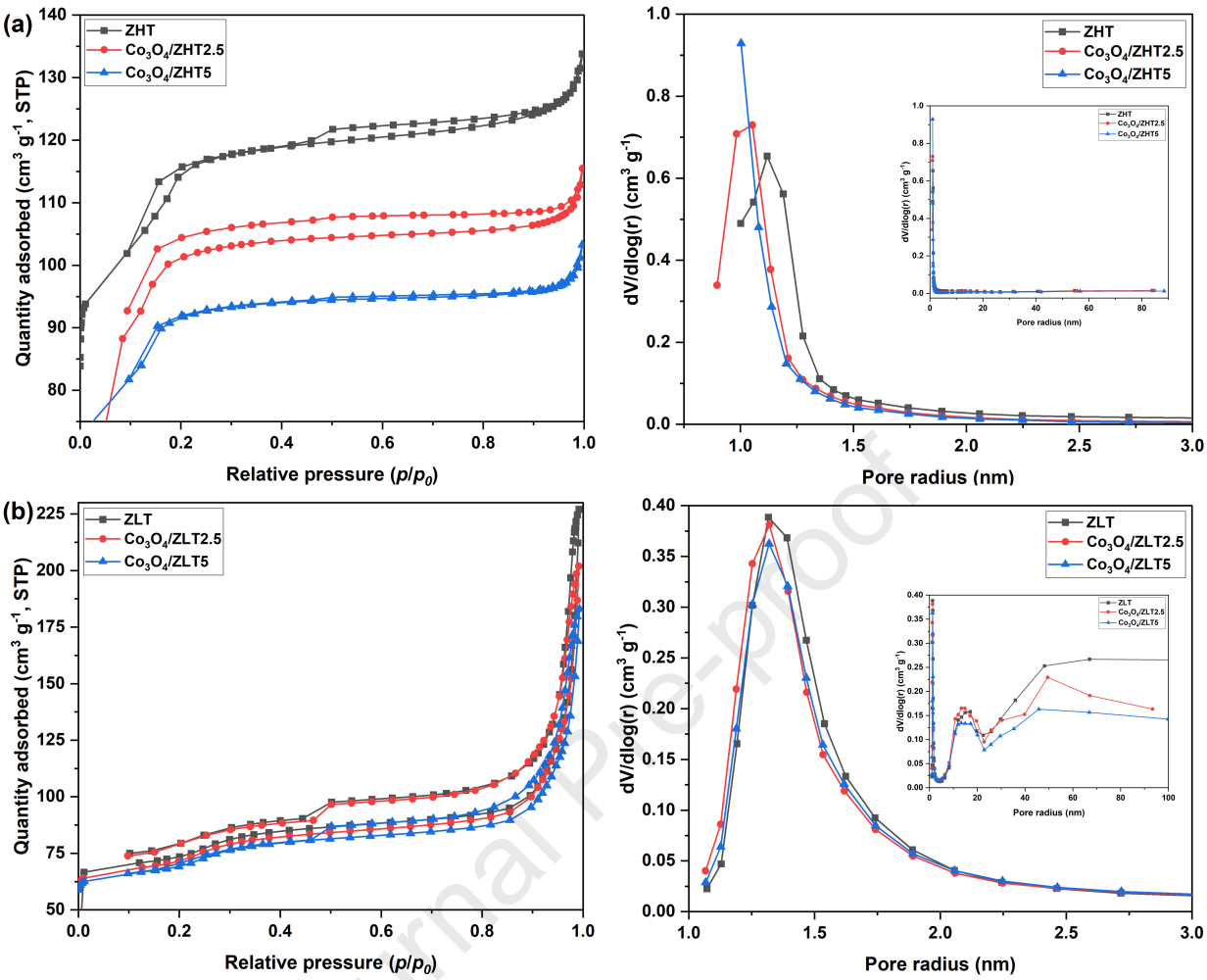

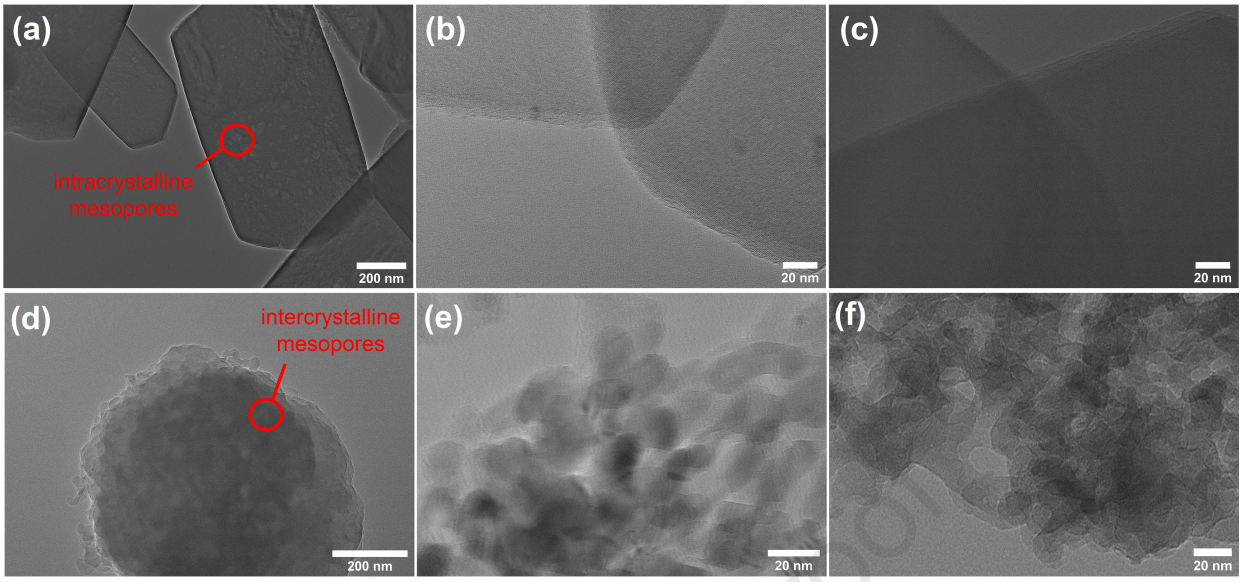

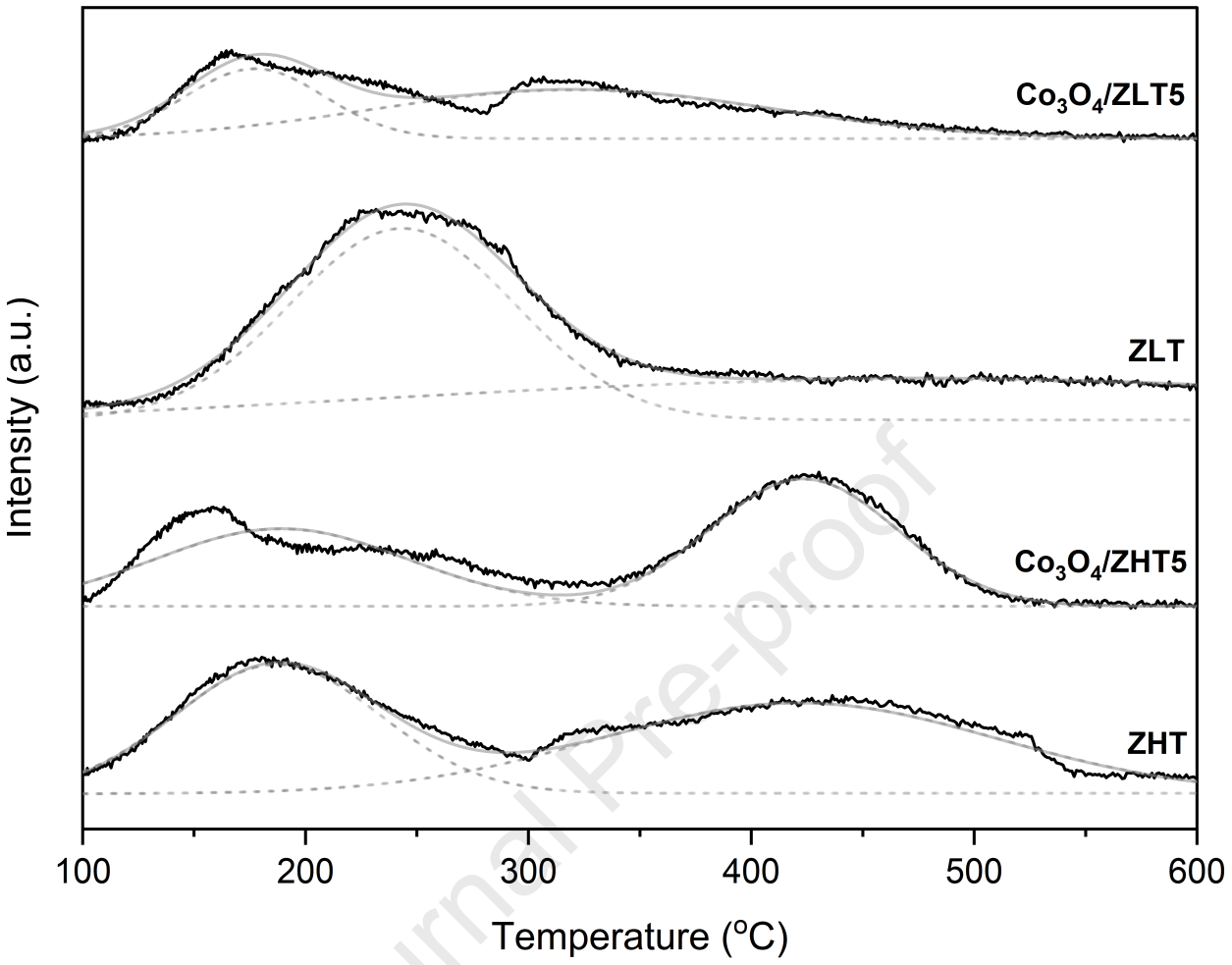

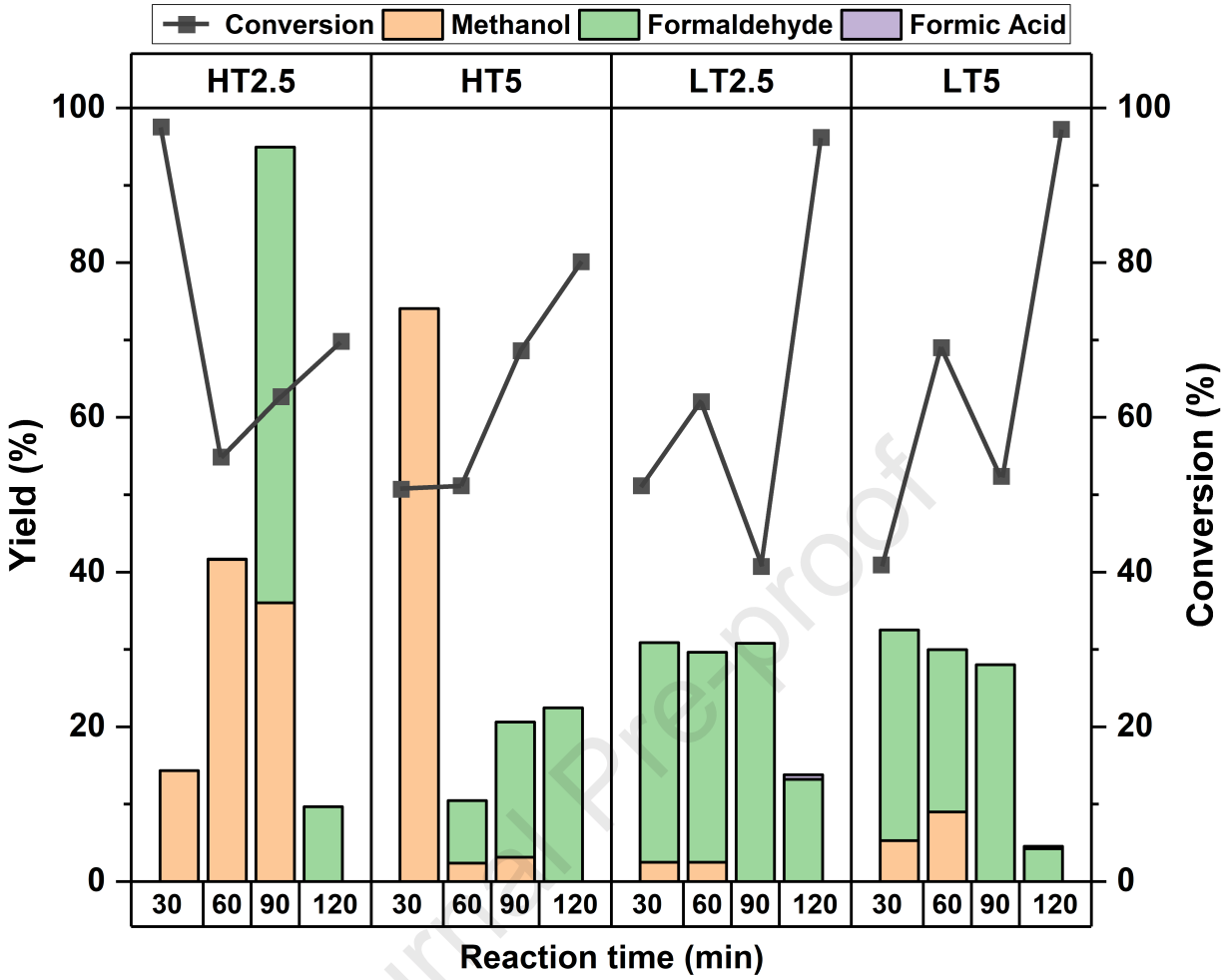

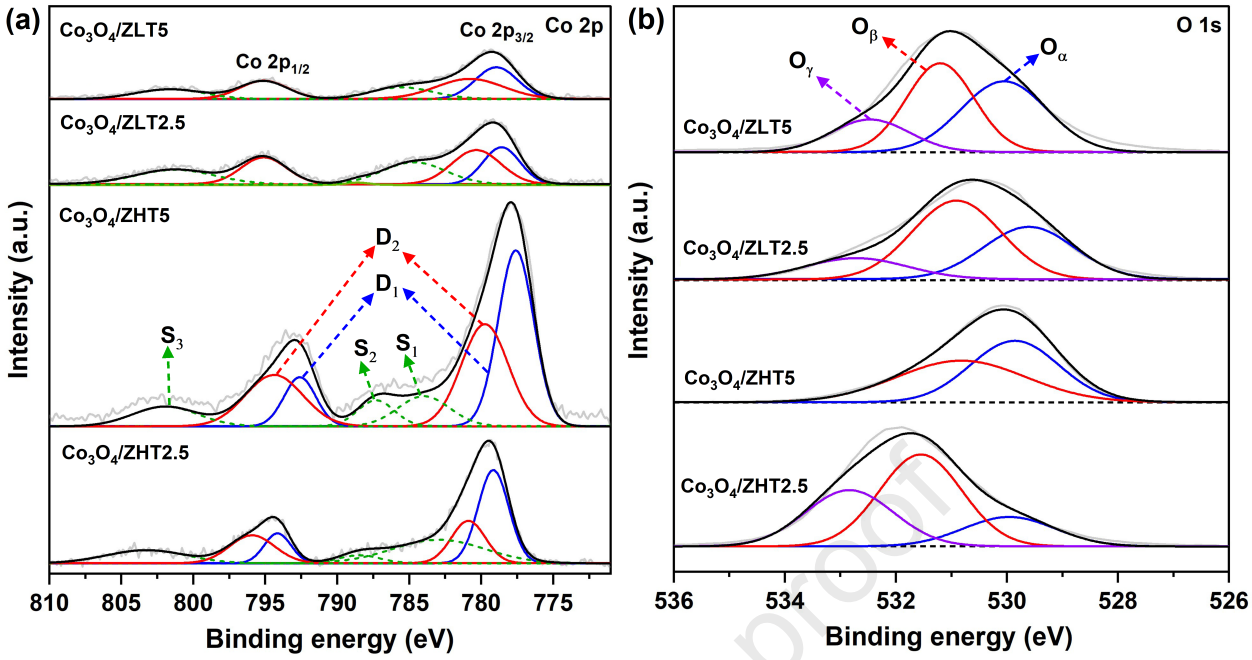

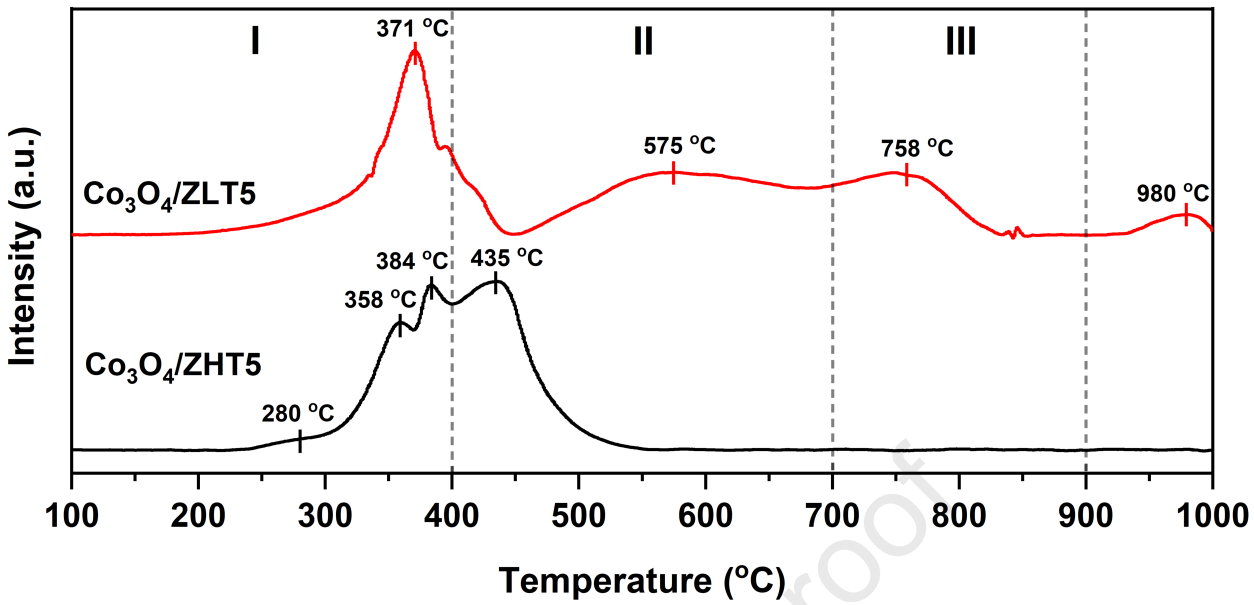

Research Highlights

- Co-oxide was impregnated on hierarchical ZSM-5 with different mesopore configurations.
- Physicochemical features were gained using methane partial oxidation as a model.
- Mesopore configuration affects porosity, Co dispersion, behavior, and reducibility.

Declaration of Competing Interest

We declare that we have no financial interests and personal relationships with other people or organizations that can inappropriately influence our work reported in this manuscript.